Design and Development of $CsSnI_3$ Solar Cell Using SCAPS-1D Simulation

by

Somayia

20315001

A thesis submitted to the Department of Mathematics and Natural Sciences
in partial fulfillment of the requirements for the degree of
Bachelor of Science in Applied Physics and Electronics

Department of Mathematics and Natural Sciences
Brac University
August 2024

Declaration

It is hereby declared that

1. The thesis submitted is my own original work while completing degree at Brac University.
2. The thesis does not contain material previously published or written by a third party, except where this is appropriately cited through full and accurate referencing.
3. The thesis does not contain material which has been accepted, or submitted, for any other degree or diploma at a university or other institution.
4. We have acknowledged all main sources of help.

Student's Full Name & Signature:

SOMAYIA

20315001

Approval

The thesis titled "Design and Optimization of CsSnI3-Based Solar Cells Using SCAPS-1D Software," submitted by Somayia (20315001) during the Fall of 2024, has been accepted as satisfactory in partial fulfillment of the requirements for the degree of Bachelor of Science in Applied Physics and Electronics, as of November 28, 2024.

Examining Committee:

Supervisor:

Md. Firoze H. Haque

Associate Professor and Chairperson
Department of Mathematics and Natural Sciences
BRAC University

Co-supervisor:

Muhammad Lutfor Rahman

Assistant Professor
Department of Mathematics and Natural Sciences
BRAC University

Head of Department:
(Chair)

Md. Firoze H. Haque

Associate Professor and Chairperson
Department of Mathematics and Natural Sciences
BRAC University

Abstract

Solar cells are popular because they offer a clean, renewable way to produce electricity from sunlight without harming the environment. Recently, lead-based perovskites have been used in the absorber layer in the construction of solar cells due to their ability to absorb light, high carrier mobility, and tunable band gap. However, lead is known to be toxic, posing safety challenges for the environment. To address this problem, extensive research is being conducted to find alternatives, such as developing safer lead-free perovskites.

This study proposes a model for a lead-free solar cell consisting of a cesium tin iodide perovskite in the absorber layer. A simulation was conducted using SCAPS-1D software, which allows users to create a model and analyze its various properties. Indium Tin Oxide (ITO) was chosen as the transparent conducting layer. [6,6]-Phenyl-C61-butyric acid methyl ester (PCBM), an organic compound, was chosen as the electron transport layer (ETL), and Copper Iron Tin Sulfide (CFTS) was used for the hole transport layer (HTL). Cesium Tin Iodide ($CsSnI_3$) was used as the absorber layer, which was sandwiched between the ETL and HTL. Lastly, gold (Au) was used to serve as contacts between the layers.

Once the device was modeled, several parameters, such as the thickness of each layer, doping concentrations, electron affinities, and temperatures, were varied to study their impact on power conversion efficiency (PCE), fill factor (FF), open-circuit voltage (Voc), and short-circuit current (Isc).

The simulation indicated that the maximum obtained power conversion efficiency stood at 26.9% for this device at a temperature of 298 K by optimizing these parameters. The results demonstrate that the device is a promising alternative to both the current market-available solar cells and lead-based perovskite solar cells.

Dedication

This thesis is dedicated to my mother, Shahana Akhter, whose unwavering support, love, and encouragement have been my constant source of strength. Her belief in me has inspired me to push beyond my limits and strive for excellence. I am deeply grateful for her sacrifices and guidance, which have played a pivotal role in helping me reach this milestone.

Acknowledgement

First and foremost, I offer my deepest gratitude to Almighty Allah for granting me the strength, resilience, and perseverance needed to complete this research.

I am profoundly grateful to my supervisors, Dr. Firoze Haque and Md. Lutfor Rahman, for their exceptional guidance and support throughout this project. Despite their demanding schedules, they always found time to help me, patiently addressing my questions and offering encouragement at every step.

I would also like to extend my sincere thanks to the faculty members of the Mathematics and Natural Sciences Department at Brac University for their constant support and encouragement. My heartfelt appreciation goes to my senior researcher, Dolon Pal, whose mentorship and guidance were instrumental in my personal and academic growth.

I am especially thankful to my friends and family for their steadfast support. A special acknowledgment goes to Fatin Salsabil Majumder, Fardin Salsabil Majumder, Isa Sayek Huda, and Haseen Hamid for being a constant source of encouragement and friendship throughout this journey.

Lastly, I am deeply indebted to my mother, Shahana Akhter, for her boundless love, sacrifices, and unwavering support. Her influence and dedication have profoundly shaped who I am, and I am forever grateful.

Table of Contents

Declaration i

Approval ii

Abstract iii

Dedication iv

Acknowledgment v

Table of Contents vi

List of Figures viii

List of Tables ix

Acronyms 1

1 Introduction 1
- 1.1 Literature Review . . . 2
- 1.2 Research Objectives . . . 3
- 1.3 Structure of the Thesis . . . 3

2 Background Theory 4
- 2.1 Understanding N-Type and P-Type Doping . . . 5
  - 2.1.1 The Photovoltaic Effect . . . 6
  - 2.1.2 The Working Principle of a Solar Cell . . . 6
  - 2.1.3 Perovskite . . . 9
  - 2.1.4 The Functioning of a Perovskite-Based Solar Cell . . . 10
  - 2.1.5 Cesium Tin Iodide . . . 11
- 2.2 Fundamental Parameters and Electrical Characterization Methods . . . 11
  - 2.2.1 Current-Voltage Characteristics of a a Photovoltaic Device . . . 11
  - 2.2.2 Open circuit voltage . . . 12
  - 2.2.3 Efficiency and Fill Factor . . . 13

3 Equations Governing Solar Cell Operation 14
- 3.1 Poisson's equation . . . 14
- 3.2 Continuity Equations . . . 15
- 3.3 Drift-Diffusion equations . . . 16
- 3.4 Recombination Mechanisms in Semiconductors . . . 17

3.4.1 Radiative Recombination . . . 17
3.4.2 Shockley-Read-Hall (SRH) Recombination . . . 18
3.4.3 Auger Recombination . . . 18
3.4.4 Surface Recombination . . . 18
3.4.5 Bimolecular Recombination . . . 19
3.5 Optical Generation in Semiconductors . . . 19
3.5.1 Photon Absorption . . . 19
3.5.2 Generation Rate . . . 19
3.5.3 Absorption Coefficient . . . 19
3.5.4 Carrier Recombination . . . 20
3.5.5 Quantum Efficiency . . . 20
3.6 Optical Generation in Solar Cells . . . 20

4 NUMERICAL ANALYSIS 21
4.1 Advancing Solar Energy Through Numerical Analysis . . . 21
4.2 Solar Cell Capacitance Simulator . . . 22
4.2.1 SCAPS-1D Interface Description . . . 23
4.2.2 SCAPS-1D Solar Cell Definition Panel . . . 24
4.2.3 Customizing Solar Cell Layer Parameters . . . 25
4.2.4 Configuring Illumination Settings . . . 25
4.2.5 Step-by-Step Simulation Process . . . 26
4.2.6 Simulated Curves . . . 27
4.2.7 Proposed CsSnI3-Based Solar Cell . . . 27
4.3 JV Characteristics and Quantum Efficiency . . . 30
4.4 Impact of ITO Thickness . . . 31
4.5 Impact of PCBM Thickness . . . 32
4.6 Impact of $CsSnI_3$ Thickness . . . 33
4.7 Impact of CFTS thickness . . . 34
4.8 Impact of Electron Affinity . . . 35
4.8.1 Impact of CFTS Electron Affinity on PCE (Graph a) . . . 35
4.8.2 Impact of PCBM Electron Affinity on PCE (Graph b) . . . 35
4.8.3 Overall Analysis . . . 36
4.9 Impact of Doping Concentration on Solar Cell parameters and Efficiency 37
4.9.1 Impact of Doping PCBM . . . 37
4.9.2 Impact of Doping CsSnI3 . . . 37
4.9.3 Impact of Doping CFTS . . . 37
4.10 Impact of Temperature on PCE . . . 39
4.11 Analysis of Optimized Result . . . 42

Bibliography 45

List of Figures

1.1 A Solar Cell Based on Perovskite Materials 1

2.1 Semiconductors and Their Position in the Periodic Table 4
2.2 Energy Band Diagrams for Metals, Insulators, and Semiconductors . 5
2.3 Doping Methods: N-Type and P-Type 5
2.4 Photovoltaic Effect 6
2.5 Movement of charges 8
2.6 Perovskite 9
2.7 Perovskite-Based Photovoltaic Cells 10

4.1 The SCAPS Front-End Interface Design 23
4.2 SCAPS solar cell definition panel 24
4.3 Solar Cell Definition Panel in SCAPS 25
4.4 Setting Illumination Conditions 26
4.5 SCAPS Operating Procedure Flowchart 26
4.6 Output Display of SCAPS 27
4.7 Band Diagram of Materials 29
4.8 (a) $J-V$ characteristics and (b) QE curves of $CsSnI_3$ devices 30
4.9 Impact of ITO Layer Thickness on Solar Cell Efficiency and Characteristics 31
4.10 Impact of PCBM Layer Thickness on Solar Cell Efficiency and Characteristics 32
4.11 Impact of $CsSnI_3$ Layer Thickness on Solar Cell Efficiency and Characteristics 33
4.12 Impact of CFTS Layer Thickness on Solar Cell Efficiency and Characteristics 34
4.13 Impact of electron affinity of (a) HTL and (b) ETL on PCE. 36
4.14 Effect of ETL Doping Concentration on Power Conversion Efficiency (PCE). 38
4.15 Effect of Varying Acceptor Doping Concentrations in the Absorber Layer on Solar Cell Performance 39
4.16 Impact of varying doping concentration of HTL on PCE. 40
4.17 Impact of varying Temperature on PCE. 41
4.18 Impact of varying Temperature on J_{SC} and V_{OC}. 41

List of Tables

1 Symbols and their explanations. x

4.1 Defining the Input Parameters for the Simulation 28
4.2 Power Conversion Efficiency (PCE) Variation with Different Electron Affinity Values 35
4.3 Power Conversion Efficiency (PCE) Variation with Different Electron Affinity Values 36

Symbol	Explanation	Unit
PCE	Power conversion efficiency	%
FF	Fill factor	%
$\boldsymbol{V_{oc}}$	Open circuit voltage	**V**
$\boldsymbol{J_{sc}}$	Short circuit current density	$\mathbf{mA/cm^2}$
$\boldsymbol{J_0}$	Diode saturation current density	$\mathbf{mA/cm^2}$
$\boldsymbol{I}$	Diode current	**A**
$\boldsymbol{I_0}$	Diode saturation current	**A**
$\boldsymbol{V_D}$	Diode voltage	**V**
$\boldsymbol{V_T}$	Thermal voltage	**V**
$\boldsymbol{E}$	Photon energy	**eV**
$\boldsymbol{\nu}$	Frequency of light	**Hz**
$\boldsymbol{c}$	Speed of light	**m/s**
$\boldsymbol{\lambda}$	Wavelength	**nm**
$\boldsymbol{V}$	Applied potential	**V**
$\boldsymbol{I_L}$	Light generated photon current	**A**
$\boldsymbol{D}$	Diffusion constant	$\mathbf{m^2/s}$
$\boldsymbol{\alpha}$	Absorption coefficient	$\mathbf{cm^{-1}}$
k	Boltzmann constant	$\mathbf{m^2kg/s^2K}$
T	Temperature	**K**
Q	Charge	**C**
$\boldsymbol{v_{th}}$	Thermal velocity of charge carriers	**m/s**
$\boldsymbol{\sigma_p}$	Capture cross section area of hole	$\mathbf{cm^2}$
$\boldsymbol{\sigma_n}$	Capture cross section area of electron	$\mathbf{cm^2}$
$\boldsymbol{E_C}$	Conduction band minimum	**eV**
$\boldsymbol{E_V}$	Valence band minimum	**eV**
$\boldsymbol{E_{fn}}$	Electron quasi-Fermi level	**eV**
$\boldsymbol{E_{fp}}$	Hole quasi-Fermi level	**eV**
$\boldsymbol{\Delta E_C}$	Conduction band offset	**eV**
$\boldsymbol{\Delta E_V}$	Valence band offset	**eV**
$\boldsymbol{N_A}$	Uniform acceptor density	$\mathbf{cm^{-3}}$
$\boldsymbol{N_D}$	Shallow uniform donor density	$\mathbf{cm^{-3}}$
$\boldsymbol{\tau_e}$	Electron lifetime	**s**
$\boldsymbol{\tau_h}$	Hole lifetime	**s**

Table 1: Symbols and their explanations.

Chapter 1

Introduction

Energy-associated problems encompass various challenges in producing, distributing, and consuming energy. Burning fossil fuels leads to global warming and pollution. To battle these challenges, solar cells provide an efficient way to convert sunlight into electricity; this method is much cleaner and more sustainable. Sunlight is also a renewable source that is abundant in nature compared to finite sources. [3]

Currently, silicon-based solar cells are used in the market, and they utilize strong, heavy elements such as aluminum. These solar cells are also more energy-intensive and costly to produce, yet they provide only 15%-20% efficiency. Therefore, much research is being conducted to find alternatives for meeting energy requirements [18]. Perovskite solar cells are flexible, cost-effective for manufacturers, and offer higher efficiency by capturing sunlight and turning it to electric current [2]; they are composed of layers, as illustrated in Figure 1.1.

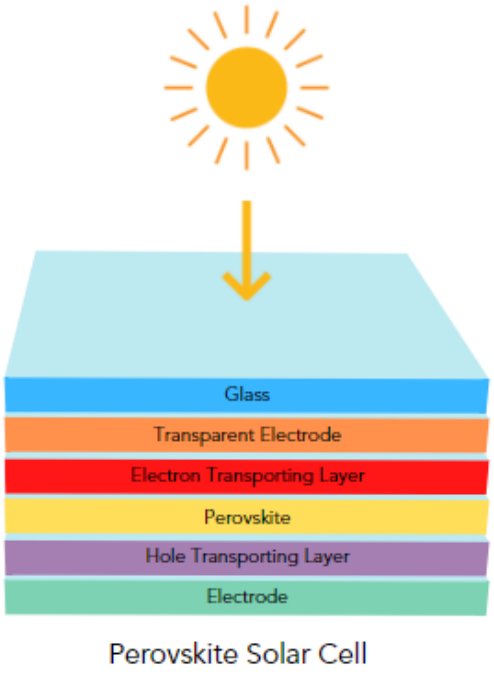

Figure 1.1: A Solar Cell Based on Perovskite Materials

1.1 Literature Review

When we think of the photovoltaic effect, we can instantly recall the Greek word "pros", which essentially means light. Moreover, named after the Italian physicist Alessandro Volta, "voltaic" refers to electricity; therefore, photovoltaic simply means converting sunlight into electrical energy. The device used for this is called a "solar cell'. A solar cell, thus, converts the light energy from the sun into electricity [3].

The photovoltaic effect was first observed by a French scientist, Edmond Becquerel, in 1839. The observation was made through an experiment in which a silver chloride electrode in acid was first connected with platinum electrodes, followed by illumination. This led to the flow of electric current in the setup, thus generating electricity; however, it was only named the Becquerel effect at that time.[12]. Later, in 1877, Adams and Day conducted a similar experiment using a metal-based solar cell and sunlight. Much research progressed over the years, but the first solar cell to be manufactured industrially for use was available in the 1950s.

In 1954, Chapin, Pearson, and Fuller introduced a solar cell model that was ready to be commercially sold. It was used in satellites orbiting the Earth to provide energy directly from sunlight. Ever since then, a lot of research has been conducted to improve the efficiency of solar cells. Today, an efficiency of a whopping 25% in solar cells is readily found experimentally; however, much lower-efficient solar cells are sold commercially. [1].

The solar cells that are available in the markets are very versatile and durable, which is also why the purchase rate has increased. Consumers have been investing in installing solar panels to power homes, schools, industries, and remote irrigation systems. All in all, the use of solar cells has significantly increased over the years across all fields for energy. As the need for energy grows, we need access to more efficient solar cells. [10].

When designing solar cells was considered, materials that were highly efficient were needed. Perovskites provide a promising alternative to the already available materials used in solar cells. These are materials that are low in cost, durable, and highly efficient, and their bandgaps can be tuned. Moreover, the additional beneficial features of perovskites, which include their light weight, ability to manufacture at low temperatures and less energy-intensive manufacturing process, make them a perfect candidate for solar cell applications. However, the problem was in attaining stability of the structure, which often required the introduction of lead in the material. As lead has toxic environmental effects, much research was conducted to obtain lead-free perovskite for solar cells. [14].

1.2 Research Objectives

i. A one-dimensional analysis of a Cesium Tin Iodide solar cell was conducted using the SCAPS-1D simulation software, with input parameters based on previously established bandgap energy values from existing research .

ii. Studying the behaviour of changes in thickness, electron affinity, doping concentrations and temperature on the solar cell parameters..

iii. Proposing a model of a highly efficient solar cell by adjusting its layers and operating it at an optimum temperature.

1.3 Structure of the Thesis

This thesis is divided into four chapters, each focusing on a distinct aspect of the research, as outlined below:

i. Chapter 1 briefly navigates through the history of solar cells as a literature review, followed by a discussion of the objectives of this research and the outline of this dissertation.

ii. In Chapter 2 we shall overview the photoelectric effect and the key paramters of a solar cell

iii. In Chapter 3 we will focus on the governing equations that regulate the operation of a solar cell

iv. Chapter 4 focuses on the simulation that was conducted using scaps software and aims to propose a highly optimized solar cell structure.

Chapter 2

Background Theory

Semiconductor material belongs to group IVA of the periodic table. These materials are found between the metals and non metals in a periodic table[20]. The behaivior of semiconductors make them suitable for usage accross various fields. [23].

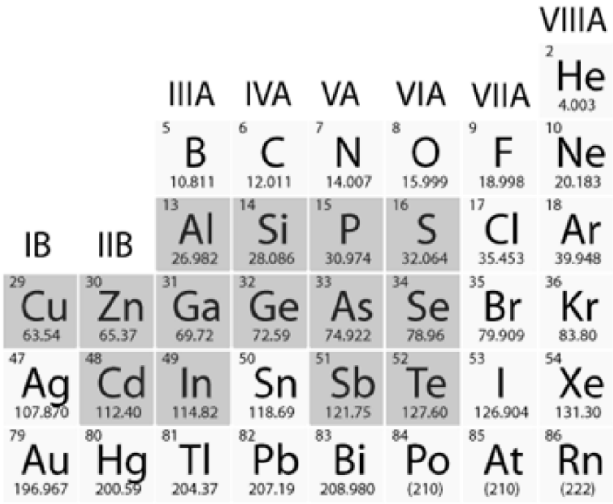

Figure 2.1: Semiconductors and Their Position in the Periodic Table

In metals, the band is overlapped; in insulators, the band gap is too large. However, in semiconductors, the band gap is intermediate between metals and insulators, which allows the electrons to jump from one band to another if provided with energy. If the band gap size is small, the electrons can easily move from the conduction band to the valence band, where they exhibit the electrical characteristics of a material as shown in 2.2. [4].

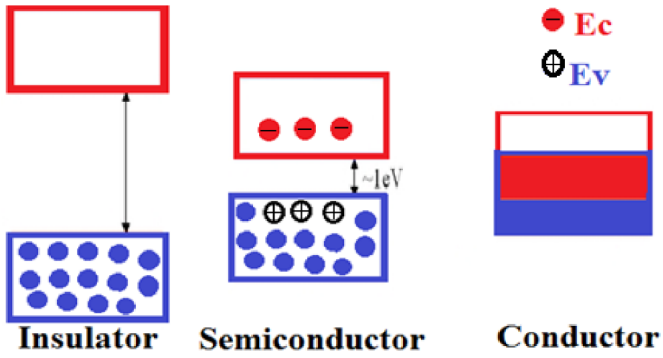

Figure 2.2: Energy Band Diagrams for Metals, Insulators, and Semiconductors

2.1 Understanding N-Type and P-Type Doping

An undoped semiconductor containing only pure atoms is referred to as an intrinsic material. However, when we intentionally introduce other materials into its structure to change its properties, we have achieved a doped sample. This can be done in two ways: N-type doping and P-type doping. In a n-type doping, the semiconductor material is introducted with elements such as phosphorus which add one or few more electrons eventually increasing the amount of electrons in the whole structure.[5]. In p-type doping, semiconductors are introduced with elements such as boron that decrease the number of electrons in the structure rather than contributing to charge carriers such as holes. The control of the amount of electrons and holes in the structure of a material drastically change the behavior of the material. [7].

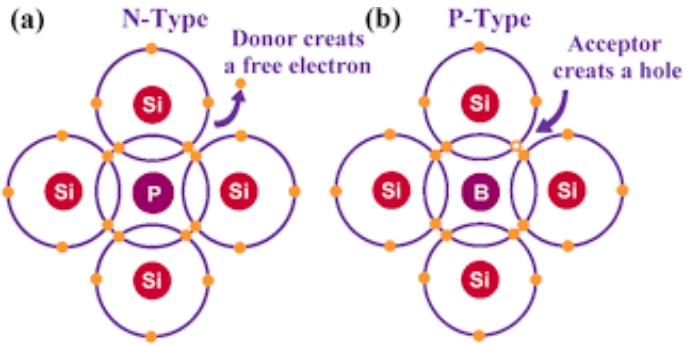

Figure 2.3: Doping Methods: N-Type and P-Type

2.1.1 The Photovoltaic Effect

When a n-type material is combined with a p-type material, a junction is formed between them, which is referred to as a P-N junction [8]. This function is deprived, where the holes have already been combined with the electrons. An electric field is set up within the material, which prevents the further movement of charge carriers. When light strikes this depletion area, the electrons are generated from the neutral atoms, which move towards the n-type material and across the circuit, generating electricity.

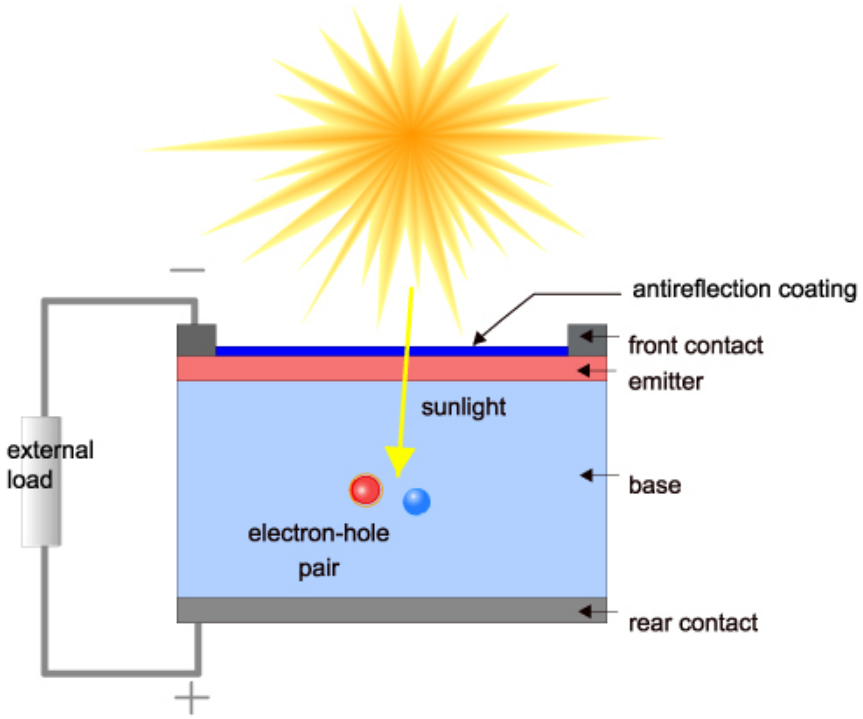

Figure 2.4: Photovoltaic Effect

2.1.2 The Working Principle of a Solar Cell

The photovoltaic effect is the core mechanism behind how solar cells generate electricity. When light hits the surface of a material, its photons are absorbed, which leads to the creation of charge carriers within the material [17]. This process is somewhat similar to the photoelectric effect, where light with a high enough frequency can cause electrons to be released from a material. In 1905, Albert Einstein offered an explanation for this phenomenon, proposing that light is made up of tiny, discrete packets of energy called photons.[19].

$$E_{ph} = h\nu \tag{2.1}$$

where

$$\nu = \frac{c}{\lambda} \tag{2.2}$$

In this context, c is the speed of light in a vacuum, which is about 3×10^8 m/s, h is the Planck's constant (6.626×10^{-34} Js), and ν is the frequency of the incoming light

that enters the material. The minimum energy required to release an electron from a material's surface, known as the work function, which is given by $\phi = hf_0$, where f_0 is the threshold frequency. When the frequency of light exceeds this threshold, electrons are knocked free from the material, a result confirmed by many experiments.
Usually, light with a frequency higher than f_0 strikes a metal electrode that's connected to the negative terminal of a battery. The second electrode is linked to the positive terminal through a potentiometer, which helps regulate the photocurrent. A galvanometer is used to measure the amount of photocurrent. The kinetic energy of the ejected electron can be expressed as:

$$K_{\max} = h\nu - \phi \tag{2.3}$$

In the equation $\phi = hf_0$ represents the work function, which is the minimum energy that is needed to release an electron from a material's surface. This occurs specifically when the frequency of the incoming light, ν, exceeds a certain threshold frequency f_0 [22]. This principle has been verified through experiments, as shown in Figure 2.13.
In the experimental setup depicted in Figure 2.13, light with a frequency greater than f_0 strikes a metal electrode (C) inside a bulb. The electrode is connected to the negative terminal of a battery, while another electrode (A) is connected to the positive terminal through a potentiometer that controls the flow of electrons. A galvanometer is used to measure the resulting photocurrent, and it is placed in series with electrode A.
In solar cells, a similar process occurs when photons strike the material, generating electrons. However, unlike the traditional photoelectric effect, these electrons remain in the material rather than being ejected. They are then captured and directed into an external circuit, known as the load, where they produce electricity. The photovoltaic effect in solar cells involves three key processes: [24].

i. Mechanisms of Photon Absorption in Photovoltaic Material

When light hits a photovoltaic (PV) material, it causes electrons to become excited and move to a higher energy state. In simpler terms, electrons in the material's valence band absorb energy from photons and jump to the conduction band, where they are free to move.
For this to happen, certain conditions must be met: the material must have available energy levels, and the energy of the incoming photon must match the gap between those levels [20].
In an ideal semiconductor, electrons only exist just below the valence band and just above the conduction band, with no states in between. If the photons have energy below the material's band gap, they simply pass through without being absorbed [15]. However, if the energy of a photon is equal to or greater than the energy gap between these bands, it excites an electron from its lower energy state to a higher state, leaving a "hole" behind in the valence band. This hole acts like a positively charged particle. The difference in energy between the conduction band (E_c) and the valence band (E_v) is called the band gap energy (E_g), which is mathematically expressed as:

$$E_g = E_c - E_v \tag{2.4}$$

ii. Charge Carrier Separation at the Junction

When electron-hole pairs are created [16], they can recombine in two main ways. In radiative recombination, electrons return to their original state and release energy in the form of light. In non-radiative recombination, however, the energy is transferred to nearby pairs rather than being emitted as light [6]. To harness this energy and power external devices, semi-permeable membranes are placed on both sides of the absorber layer. These membranes capture the energy stored in the electron-hole pairs, drawing electrons from one side and holes from the other, as shown in Figure 2.5.

The membranes are made from p-type and n-type materials, which naturally separate the electrons and holes, as illustrated in the figure. The solar cell is designed so that the charge carriers—electrons and holes—reach their respective membranes before they have a chance to recombine. The design ensures that the time it takes for the charge carriers to reach their membranes is shorter than the time it would take for them to recombine. To achieve this, the thickness of the absorber material is carefully adjusted in high-efficiency solar cells [25].

iii. Harvesting and Converting Light Energy in Solar Cells

Electrical contacts or otherwise known as terminals are used to capture the charge carriers generated by light, which therefore enables the flow of energy into an external circuit [21]. In the last part of the process involves converting that light energy into usable electrical energy. Once the charge carriers have moved through the external circuit, the electrons eventually recombine with the holes, both at the back contact and at the interface of the absorber layer. 2.5.

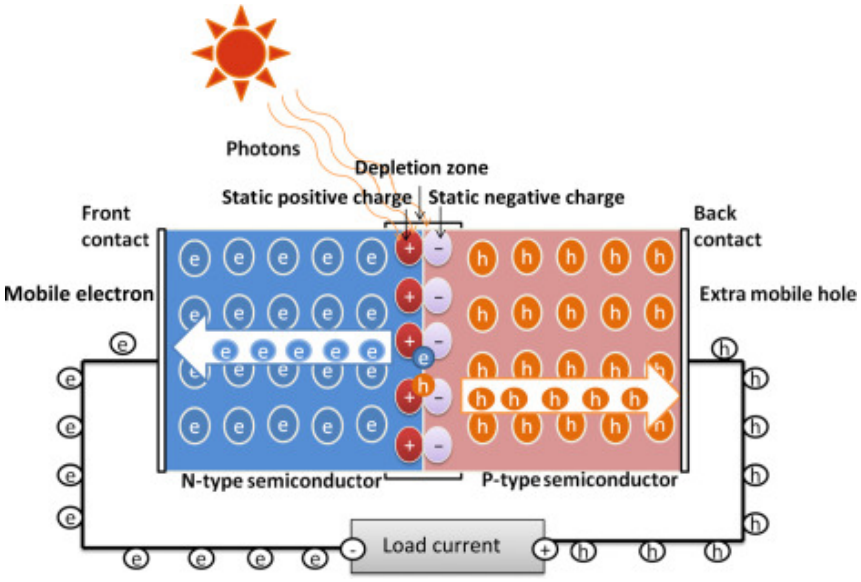

Figure 2.5: Movement of charges

2.1.3 Perovskite

Perovskites are a class of materials that can be classified as crystals. These crystals have a similar structure to calcium titanium oxide. Over the years, these materials have proven to be advantageous for many applications. we shall be particularly focusing on the benefits concerning photovoltaic applications. Perovskite materials can be flexible and easy to manufacture, thus coming at a lower manufacturing cost. The band gaps of these materials can be tuned to meet the specific purpose by carefully choosing our perovskite and doping it. Perovskite materials also prove to be highly efficient in converting sunlight to electricity. [11].

Perovskites, however, can be made using simpler processes like solution processing,

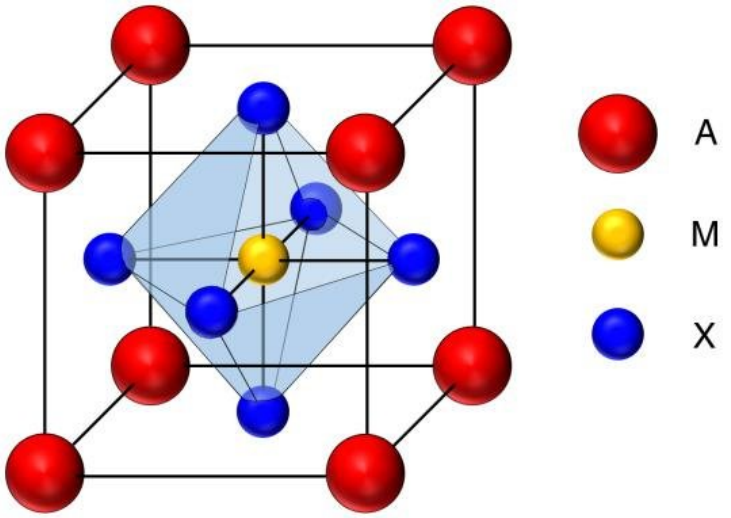

Figure 2.6: Perovskite

which could make solar power more affordable in the future [14]. While this is a huge step forward, there are still some hurdles to overcome, particularly when it comes to the durability of these cells are difficult to attain. Exposure to moisture or high temperatures can cause them to degrade, impacting their long-term performance. Another concern is that some perovskite materials contain lead, which raises environmental and safety issues. As a result, there's a push to develop lead-free alternatives. Despite these challenges, perovskites are still seen as a promising technology for solar energy and beyond, though much work remains to improve their stability and reduce their environmental footprint [13].

2.1.4 The Functioning of a Perovskite-Based Solar Cell

A perovskite solar cell generates electricity by harnessing sunlight through a specially designed perovskite layer. Here's how it works:

i. **Electron-Hole Pair Dynamics in Perovskites**: When sunlight hits the perovskite layer, it causes the excitation of the electrons in the material, leading them to jump to a higher energy level. This leaves behind "holes" in the lower energy levels, creating pairs of electrons and holes that can now move around [9].

ii. **Separation of Charges**: To generate electricity, these electrons and holes need to be separated. In perovskite solar cells, this happens naturally because the perovskite layer is positioned between two special layers: the electron transport layer (ETL) that collects electrons, and the hole transport layer (HTL) that collects holes.

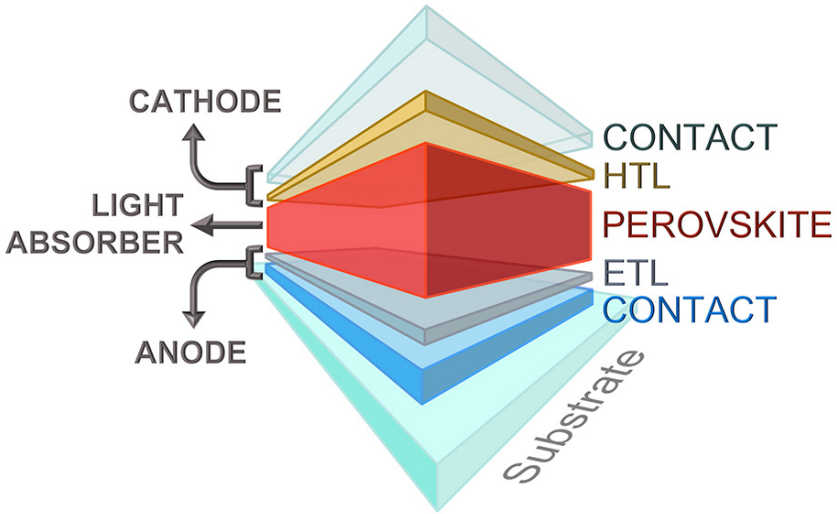

Figure 2.7: Perovskite-Based Photovoltaic Cells

iii. **Movement of Charges**: After separation, the electrons are pulled toward the ETL, and the holes move toward the HTL. The ETL guides the electrons to one side of the cell, and the HTL directs the holes to the other side.

iv. **Generating Electricity**: Once the electrons and holes reach their respective layers, they are collected by the cell's electrodes. The electrons move toward the cathode, and the holes are drawn to the anode. This movement creates an electric current as they flow through an external circuit.

v. **Power Generation**: As the electrons and holes continue to flow through the circuit, electricity is generated, which can either power devices directly or be sent to the grid for wider distribution.

2.1.5 Cesium Tin Iodide

The structure of **$CsSnI_3$** (Cesium Tin Iodide) is based on the perovskite crystal structure, which is often described by the formula **ABX_3**. For **$CsSnI_3$**, this means:

i. The **A** position is filled by **Cesium (Cs^+)**, a large positively charged ion that sits at the corners of the cubic unit cell.

ii. The **B** position is occupied by **Tin (Sn^{2+})**, a smaller metal ion located in the center of the octahedral framework.

iii. The **X** position is taken up by **Iodine (I^-)**, a negatively charged ion that forms bonds with the tin atoms, completing the octahedral coordination around each tin ion.

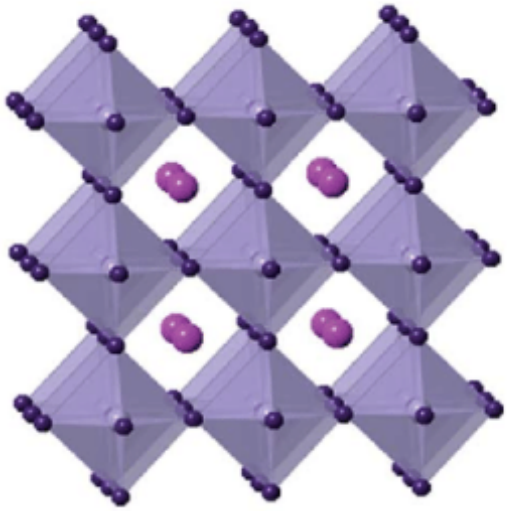

$CsSnI_3$

2.2 Fundamental Parameters and Electrical Characterization Methods

2.2.1 Current-Voltage Characteristics of a a Photovoltaic Device

The **IV characteristics curve** of a photovoltaic (PV) device is a graph that shows how a solar cell behaves under different conditions. It tells us how the solar cell's internal diode works when there's no light (dark) and when it's exposed to light (illuminated). In the dark, the solar cell acts like a typical diode, meaning it doesn't produce electricity. But when light hits the solar cell, it starts generating electrical power, and the IV curve shifts into the fourth quadrant. How far this shift goes

depends on how much light is hitting the cell. Essentially, the light adds to the current that would already be present in the dark, changing how the diode behaves. This change can be captured using the following equation:

$$I = I_0 \left[\exp\left(\frac{qV}{nkT}\right) - 1 \right] - I_L \quad (2.6)$$

where:

- I_0: This is the current that leaks through the diode when no light is present, often referred to as the "dark saturation current" [7].
- I_L: This is the current produced by the sunlight hitting the cell.
- q: This represents the charge of an electron, which is a fundamental unit in electricity.
- V: This is the voltage applied across the solar cell's terminals.
- n: This is the ideality factor, which helps us understand how the diode behaves in real-life conditions, rather than under perfect circumstances.
- k: This is Boltzmann's constant, a number that connects temperature with energy.
- T: This is the temperature of the solar cell, usually measured in Kelvin.

2.2.2 Open circuit voltage

The **open circuit voltage** (V_{oc}) is the maximum voltage that a solar cell can produce. This happens when the solar cell is not connected to anything, meaning there's no load attached. In this "open-circuit" state, the current is zero, but the voltage hits its highest point. You can calculate the open circuit voltage by setting the current to zero in the solar cell's equation, like this:

$$V_{oc} = \frac{nkT}{q} \ln\left(\frac{I_L}{I_0} + 1\right) \quad \text{at } I = 0 \quad (2.7)$$

The equation shows that V_{oc} is influenced by two things: the current generated by the light (I_L) and the saturation current (I_0), which is linked to how much recombination occurs inside the solar cell. So, V_{oc} can actually give us some insight into how much recombination is taking place in the cell. You can also see a graph of the open circuit voltage in Figure 2.17.

2.2.3 Efficiency and Fill Factor

The efficiency of a solar cell tells us how well it converts sunlight into usable electricity. It's essentially the ratio of the energy output (how much power the cell generates) to the energy input (the sunlight it absorbs). For solar cells, this efficiency is typically measured between zero and the **open-circuit voltage** (V_{oc}), which is where the cell is producing its maximum possible power. The maximum output power of a solar cell is given by this equation:

$$P_{\max} = J_{\max} V_{\max} \quad (2.8)$$

In this case, $P_{\max}$ represents the peak power, which occurs at the **maximum power point**—the point where the solar cell is working most efficiently. You can see this in Figure 2.17. The solar cell's efficiency is calculated using the following formula:

$$\eta = \frac{J_{\max} V_{\max}}{P_S} \quad (2.9)$$

Where P_S refers to the amount of power coming from the sunlight.
Now, we can also think about the solar cell's efficiency in terms of something called the **fill factor (FF)**. The fill factor helps us understand how close the solar cell is to reaching its theoretical maximum performance. It's the ratio of the actual power the cell generates to the maximum power it could theoretically generate if everything worked perfectly. You can picture this as the area of the power curve at the maximum power point compared to the theoretical area representing maximum power, which is shown in Figure 2.17.
The fill factor (FF) is given by:

$$FF = \frac{J_{\max} V_{\max}}{J_{oc} V_{oc}} \quad (2.10)$$

By rearranging this equation, we can express $J_{\max} V_{\max}$ as $FF \times J_{oc} V_{oc}$, and then...

Chapter 3

Equations Governing Solar Cell Operation

In this chapter, we shall discuss the key physics equations that will be employed during our analysis of the solar cell. The software that has been used for simulations is called SCAPS-1D (Solar Cell Capacitance Simulator). It uses many equations to calculate the amount of charge generation, transport, and recombination in solar cells. In SCAPS, these are solved numerically across the device layers, incorporating boundary conditions, material parameters, and incident light properties. We shall also discuss the impact of losses on the efficiency of the solar cell.

3.1 Poisson's equation

Poisson's equation is a crucial concept that is needed for understanding how electric fields behave in materials like the ones used in solar cells as well as our modelled solar cell. It helps us determine how the electric potential changes within the material based on how charges are distributed. The equation is below:

$$\frac{d^2\phi}{dx^2} = -\frac{\rho}{\epsilon}$$

Here, ϕ is the electric potential, ρ represents the charge density which refers to the electrons, holes, and fixed charges from the material's doping levels, and ϵ is the permittivity of the material, that tells us about how it responds to electric fields. Essentially, Poisson's equation connects the distribution of charges in a semiconductor to the electric potential and the electric field.

In a solar cell, understanding how the electric potential is distributed within the material is essential for determining how the electric field behaves. The electric field, which dictates how charge carriers (electrons and holes) move, is derived from the potential by:

$$E = -\frac{d\phi}{dx}$$

This electric field plays a critical role in separating the electron-hole pairs that are created when light hits the solar cell. These pairs need to be driven to different

sides of the cell so that they don't recombine and waste the energy. The electric field does this by pushing the electrons toward the n-side and the holes toward the p-side, where they can be collected and generate a current.

When we bring a p-type and a n-type material together, a depletion region forms between them where there are no free charge carriers. This happens because the electrons and holes recombine from both the regions, leaving behind charged ions from the doping process. The built-in electric field in this region, which is calculated using Poisson's equation, helps to prevent further recombination and ensures that the separated carriers are pushed to the electrodes.

When we think of designing solar cells, we begin with solving Poisson's equation for accurately modeling how the electric potential and electric field behave across the device. Simulating these properties using software tools allows us to predict how changes in material properties, doping levels, and other factors will impact performance. By doing this, they can optimize the design to create more efficient solar cells.

The electric field generated by Poisson's equation also helps reduce losses due to recombination, which occurs when electrons and holes come back together before they can be collected. By driving the carriers toward the electrodes, the electric field increases the chances that they will contribute to the current instead of recombining.

3.2 Continuity Equations

The continuity equations describe how charge carriers—electrons and holes—move through semiconductors, focusing on how they are created, recombine, and spread out. These factors are crucial for the functioning of solar cells, as they impact how efficiently the carriers can generate electricity and how much energy is lost when they recombine.The continuity equations for electrons and holes are expressed as:

$$\frac{\partial n}{\partial t} = \nabla \cdot (D_n \nabla n) + G_n - R_n$$

$$\frac{\partial p}{\partial t} = \nabla \cdot (D_p \nabla p) + G_p - R_p$$

Where:

- $n(x,t)$ is the electron concentration (number of electrons per unit volume),
- $p(x,t)$ is the hole concentration (number of holes per unit volume),
- D_n and D_p are the diffusion coefficients for electrons and holes, respectively,
- G_n and G_p represent the generation rates of electrons and holes (e.g., from light absorption),
- R_n and R_p are the recombination rates of electrons and holes.

Carrier diffusion helps us understand how charge carriers, such as electrons and holes, naturally move from the areas in which they are in higher concentrations to areas with lower concentrations due to thermal motion. The terms $\nabla \cdot (D_n \nabla n)$ and $\nabla \cdot (D_p \nabla p)$ in the continuity equations capture this process, where the gradient operator ∇ indicates how the carrier concentration changes spatially, and D_n and D_p represent the ease with which electrons and holes diffuse in the material.

Carrier generation occurs when energy, typically from light or heat, creates new charge carriers. In solar cells, this process is driven by photons from sunlight, which generate electron-hole pairs. The terms G_n and G_p in the equations represent the rate of this generation.

On the hand, carrier recombination happens when electrons and holes combine within the material itself and effectively cancel each other out, reducing the number of free carriers that contribute to current. The terms R_n and R_p describe this recombination process. Recombination can happen in different ways:

- **Radiative recombination**: Electrons and holes recombine, releasing energy in the form of light.
- **Shockley-Read-Hall (SRH) recombination**: Carriers recombine through trap states in the material, often due to imperfections or impurities.
- **Auger recombination**: In this case, three carriers interact, with one gaining energy from the others and causing recombination.

The partial derivatives $\frac{\partial n}{\partial t}$ and $\frac{\partial p}{\partial t}$ indicate how the concentration of electrons and holes changes over time, as they are influenced by generation, recombination, and diffusion.

When a system reaches steady-state conditions, carrier concentrations no longer change over time. In this state, the continuity equations show a balance between the processes of generation, recombination, and diffusion. However, in transient conditions, where the system is still evolving (such as with fluctuating light intensity or temperature), the carrier concentrations continue to change, and the time derivatives stay nonzero.

3.3 Drift-Diffusion equations

The **drift-diffusion equations** describe how charge carriers (electrons and holes) move through semiconductor materials due to two main factors: electric fields and concentration gradients.

- **Drift**: The movement of carriers caused by the electric field, which pushes electrons and holes in opposite directions. For electrons, this is represented as $q\mu_n n\mathbf{E}$, and for holes, it is $q\mu_p p\mathbf{E}$, where μ_n and μ_p are the mobilities of electrons and holes, and $\mathbf{E}$ is the electric field.

- **Diffusion**: The process where carriers move from areas of high concentration to low concentration, represented by $-qD_n\nabla n$ for electrons and $-qD_p\nabla p$ for holes. Here, D_n and D_p are diffusion coefficients, and n and p are the concentrations of electrons and holes.

Together, these processes determine the current density of electrons and holes in the material:

$$\mathbf{J}_n = -qD_n\nabla n + q\mu_n n\mathbf{E}$$

$$\mathbf{J}_p = -qD_p\nabla p + q\mu_p p\mathbf{E}$$

These equations help explain how charge carriers move through semiconductors under different conditions. In devices like solar cells, the drift-diffusion equations are crucial for understanding how sunlight-generated electron-hole pairs are transported and how efficiently they can contribute to current generation. When combined with continuity equations, they provide a complete picture of how carriers are generated, moved, and recombined within the device.

3.4 Recombination Mechanisms in Semiconductors

Recombination in semiconductors occurs when electrons and holes combine, reducing the number of charge carriers that can contribute to current. This is particularly important in devices like solar cells, where high carrier concentrations are necessary for efficient energy conversion. Below are the main recombination mechanisms:

3.4.1 Radiative Recombination

Radiative recombination occurs when an electron in the conduction band recombines with a hole in the valence band, releasing energy in the form of light (photon). Although this process is utilized in light-emitting devices like LEDs, it is a loss mechanism in solar cells because the emitted light cannot be used to generate current.
The recombination rate is given by:

$$R_{\text{rad}} = \beta_{\text{rad}} np$$

where:

- β_{rad} is the radiative recombination coefficient,
- n and p are the electron and hole concentrations, respectively.

3.4.2 Shockley-Read-Hall (SRH) Recombination

SRH recombination occurs via defect states or traps within the semiconductor's bandgap. These defects capture electrons or holes, allowing recombination to occur without emitting a photon, typically releasing the energy as heat.
The recombination rate for SRH is:

$$R_{\text{SRH}} = \frac{np - n_i^2}{\tau_p \left(1 + \frac{n}{n_t}\right) + \tau_n \left(1 + \frac{p}{p_t}\right)}$$

where:

- n_i is the intrinsic carrier concentration,
- τ_p and τ_n are the hole and electron lifetimes, respectively,
- n_t and p_t are the trap densities for electrons and holes, respectively.

3.4.3 Auger Recombination

In Auger recombination, the energy released during recombination is transferred to a third carrier, which is excited to a higher energy state. This mechanism becomes significant at high carrier concentrations.
The recombination rate is:

$$R_{\text{Auger}} = C_{\text{Auger}} n^2 p$$

where:

- C_{Auger} is the Auger recombination coefficient,
- n and p are the electron and hole concentrations.

3.4.4 Surface Recombination

At the surface of a semiconductor, where atoms are not fully bonded, recombination centers are more abundant, increasing the likelihood of carrier recombination. This process, called surface recombination, is particularly significant in thin-film devices.
The surface recombination rate is:

$$R_{\text{surf}} = \frac{n_s}{\tau_{\text{surf}}}$$

where:

- n_s is the surface carrier density,
- τ_{surf} is the surface recombination lifetime.

3.4.5 Bimolecular Recombination

This type of recombination involves the direct annihilation of an electron and a hole in the bulk material. The recombination rate is proportional to the product of electron and hole concentrations.
The recombination rate is:

$$R_{\text{bimol}} = \beta_{\text{bi}} np$$

where:

- β_{bi} is the bimolecular recombination coefficient,
- n and p are the electron and hole concentrations.

3.5 Optical Generation in Semiconductors

Optical generation occurs when photons are absorbed by a semiconductor, exciting electrons from the valence band to the conduction band, thus creating electron-hole pairs. These carriers are crucial for generating electrical current, especially in devices like solar cells.

3.5.1 Photon Absorption

For a photon to create an electron-hole pair, its energy E_γ must be greater than or equal to the material's bandgap energy E_g. In direct bandgap semiconductors, this transition is straightforward, but for indirect bandgap materials (such as silicon), an additional interaction with phonons is required.

3.5.2 Generation Rate

The rate at which electron-hole pairs are created depends on both the light intensity and the material's ability to absorb photons. This can be expressed as:

$$G(\mathbf{r}, t) = \alpha(\mathbf{r}) I(\mathbf{r}, t)$$

where $\alpha(\mathbf{r})$ is the material's absorption coefficient, and $I(\mathbf{r}, t)$ is the intensity of incident light.

3.5.3 Absorption Coefficient

The absorption coefficient α describes how effectively a material absorbs light at different photon energies. It often follows a formula like:

$$\alpha(E_\gamma) = \frac{A}{E_\gamma - E_g}$$

where A is a material constant, and E_γ is the energy of the incoming photon.

3.5.4 Carrier Recombination

Once generated, the electron-hole pairs must survive long enough to be collected. If they recombine (when an electron and hole meet), they are lost. The rate of recombination is given by:

$$R = \frac{np - n_i^2}{\tau_p \left(1 + \frac{n}{n_t}\right) + \tau_n \left(1 + \frac{p}{p_t}\right)}$$

where n and p are the concentrations of electrons and holes, and τ_p, τ_n are their respective lifetimes.

3.5.5 Quantum Efficiency

Quantum efficiency is a measure of how effectively absorbed photons lead to the generation of carriers. It is given by:

$$\eta_{\text{optical}} = \frac{\text{Carriers generated}}{\text{Photons absorbed}}$$

3.6 Optical Generation in Solar Cells

In solar cells, optical generation is driven by sunlight, where photons generate electron-hole pairs. The efficiency of this process depends on factors such as the material's absorption properties, the lifetime of the carriers before recombination, and the efficiency of carrier collection.

Chapter 4

NUMERICAL ANALYSIS

4.1 Advancing Solar Energy Through Numerical Analysis

In today's world of research, computer simulations and virtual environments have become one of the essential tools for solving problems. By using computational methods, we are able understand complex challenges more effectively and find innovative solutions. This approach not only saves time but also allows for extensive testing and fine-tuning of designs in a virtual spaces, reducing the need for costly physical prototypes that can be difficult to build. These advantages are why many institutions are now using various softwares. This shift has been particularly impactful in fields like semiconductor technology, which powers devices we use daily, such as smartphones, laptops, and solar panels. Solar cells, for instance, offer a greener, more sustainable energy source by converting sunlight into electricity.

Despite the growing potential of solar energy, much of the world still depends on traditional energy sources like coal, hydropower, and nuclear power. Unfortunately, burning fossil fuels leads to significant environmental problems, which makes the search for renewable alternatives all the more urgent. While solar cells have reached efficiency levels of up to 22%, challenges like high costs and ensuring long-term durability remain obstacles. Numerical analysis through computer models has become an invaluable tool for addressing these issues. By testing designs virtually, researchers can save time and gain deeper insights compared to manual methods, all without the need for physical prototypes.

This ability to use numerical analysis has proven to be a game-changer for improving solar cell technology. Researchers can evaluate how well a proposed design might work by analyzing important factors such as the thickness of the layers, the concentration of dopants, and the effect of temperature. To achieve accurate results, it's crucial to have a reliable baseline for comparison. This helps researchers predict how a design will perform and determine whether it's a viable option for real-world applications.

4.2 Solar Cell Capacitance Simulator

SCAPS-1D, short for Solar Cell Capacitance Simulator, is a highly regarded software tool designed to simulate solar cells in a one-dimensional framework. Developed at Ghent University's Department of Electronics and Information Systems (ELIS) in Belgium, it has become a trusted resource for researchers, offering a wide range of features to support advanced solar cell analysis. One of its key strengths is the ability to model up to seven distinct semiconductor layers, making it highly versatile for diverse solar cell designs.
The latest release, SCAPS version 3.3.10, introduces several advanced features:

- **Versatile Layer Modeling**: SCAPS-1D can model up to seven distinct semiconductor layers, making it adaptable for a variety of solar cell designs.
- **Comprehensive Physical Parameters**: Includes key parameters such as bandgap energy (E_g), electron affinity (χ), dielectric constant (ϵ), doping concentrations (N_A, N_D), and defect densities (N_t) for accurate and detailed simulations.
- **Advanced Recombination Mechanisms**: Simulates crucial processes like Shockley-Read-Hall (SRH) and Auger recombination, vital for understanding energy losses.
- **Customizable Defects**: Allows precise definition of defect densities, charge states (neutral, singly/doubly charged donors or acceptors), and energy distributions (uniform levels, Gaussian distributions, single levels, and band tail states).
- **Electrode and Illumination Flexibility**: Supports defining electrode work functions, optical filters, and simulating illumination with various spectra (AM0, AM1.5D, AM1.5G, monochromatic, and white light). Includes options for front or back contact illumination and cutoff filters.
- **Detailed Output Metrics**: Generates extensive analytical outputs such as energy band diagrams, current-voltage curves, capacitance-voltage profiles, quantum efficiency, and recombination data under different temperature conditions.
- **Batch Simulation and Scripting**: Enables batch processing for systematic studies and offers scripting capabilities for enhanced control over simulations.
- **User-Friendly Design**: Features an intuitive interface, supports saving customized settings, and provides ease of use even for complex simulations.
- **Integrated Curve-Fitting Tool**: Simplifies data analysis and interpretation, aiding researchers in deriving meaningful insights.
- **Research Flexibility and Precision**: Combines robust modeling, advanced customization, and detailed analytical outputs, making it ideal for exploring innovative solar cell designs and improving their performance.

4.2.1 SCAPS-1D Interface Description

Figure 4.1 illustrates the main interface of the SCAPS-1D software, we discuss an overview of each section below:

- **Section 1 (Green Box)** Defines simulation parameters, manages files, and provides tools for saving, recording results, and generating graphs.
- **Section 2 (Blue Box)** Configures simulations like I-V, C-V, C-F, and QE. Customizes voltage, frequency, and wavelength settings.
- **Section 3 (Orange Box)** Sets illumination parameters, including light spectra (e.g., AM1.5G) and optical properties for "Dark" or "Light" modes.
- **Section 4 (Purple Box)** Adjusts series (R_s) and shunt (R_{sh}) resistances and manages action lists and saved settings.
- **Bottom Section (Gray Buttons)** Provides buttons for running simulations, batch processing, curve fitting, and scripting.

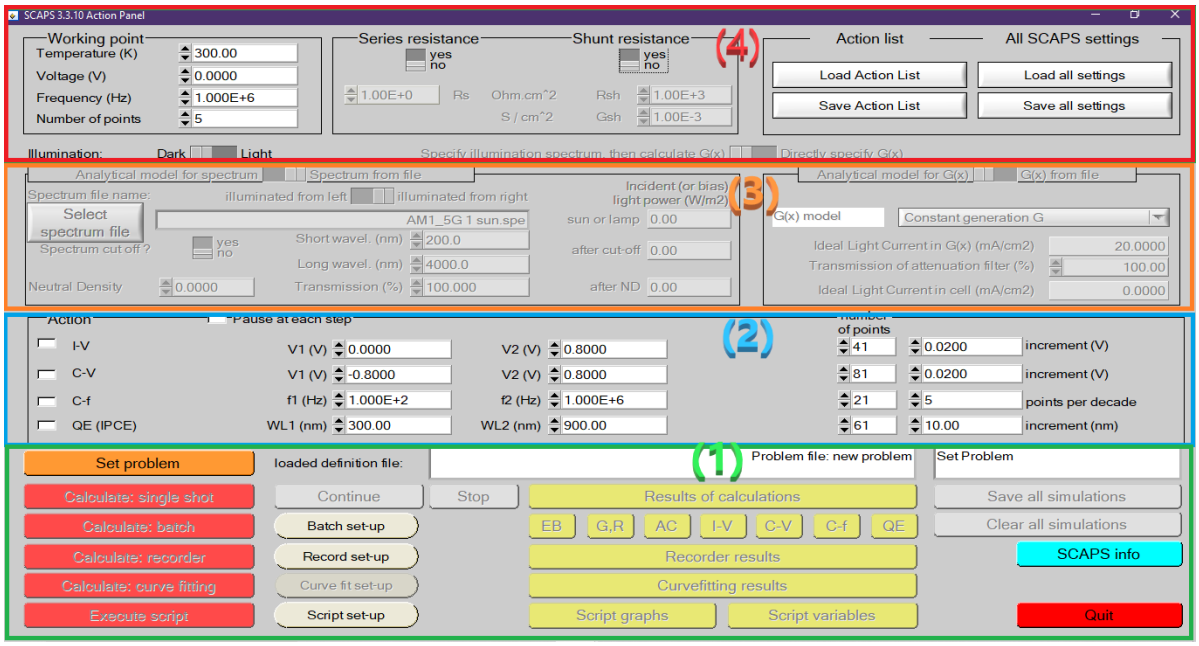

Figure 4.1: The SCAPS Front-End Interface Design

4.2.2 SCAPS-1D Solar Cell Definition Panel

This panel plays a vital role in managing both the structural setup and the graphical representation of the solar cell. For ease of use, it is divided into three primary sections, as illustrated in Figure 4.2.

i. **Section 1 (Blue Box): Layers and Interfaces**:

- Define the layers of the solar cell structure (e.g., ITO, PCBM, CsSnI3, CFTS).
- Add or remove layers using the "add layer" option.
- Configure interfaces between layers.
- Access the **numerical settings** for advanced parameter adjustments.
- Displays graded parameter information (available only after a calculation).

ii. **Section 2 (Green Box): Visualization Panel**:

- Provides a visual representation of the solar cell structure with color-coded layers.
- Options to control illumination direction: Illuminate from the **Front** or **Back**.
- Voltage application settings: Apply voltage to the **Left Contact** or **Right Contact**.
- Current reference modes: Set to **Consumer** or **Generator**.
- **Invert structure** button to reverse the layer order for analysis.

iii. **Section 3 (Orange Box): Problem Management**:

- Create a new solar cell structure using the **New** button.
- Load an existing solar cell definition using the **Load** button.
- Save the current configuration with the **Save** button.
- Use the **OK** button to confirm changes or **Cancel** to discard them.

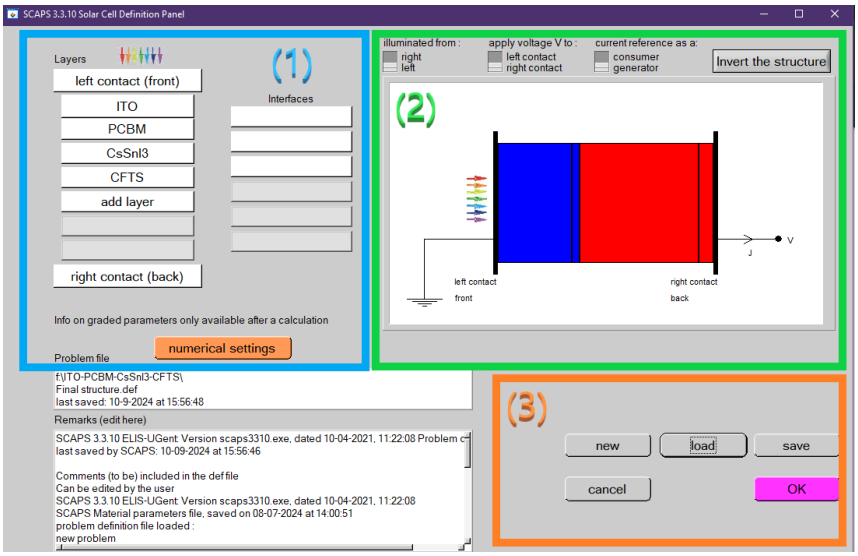

Figure 4.2: SCAPS solar cell definition panel

4.2.3 Customizing Solar Cell Layer Parameters

Figure 4.2 shows the SCAPS-1D Layer Properties Panel, where users can define and customize the properties of a solar cell layer. The left section includes options to set thickness, doping type (p-type or n-type), doping concentration, and material properties such as bandgap energy, electron affinity, dielectric constant, and mobility values.

The middle section allows configuration of recombination mechanisms, including band-to-band, radiative, and Auger recombination, with input fields for corresponding coefficients.

The right section focuses on defect management, enabling users to add, edit, or remove defects and specify their type, energy levels, and capture cross-sections, with a summary displayed below.

At the bottom, buttons provide options to save or load material data, or accept and apply changes, making the panel a comprehensive tool for tailoring solar cell layer properties.

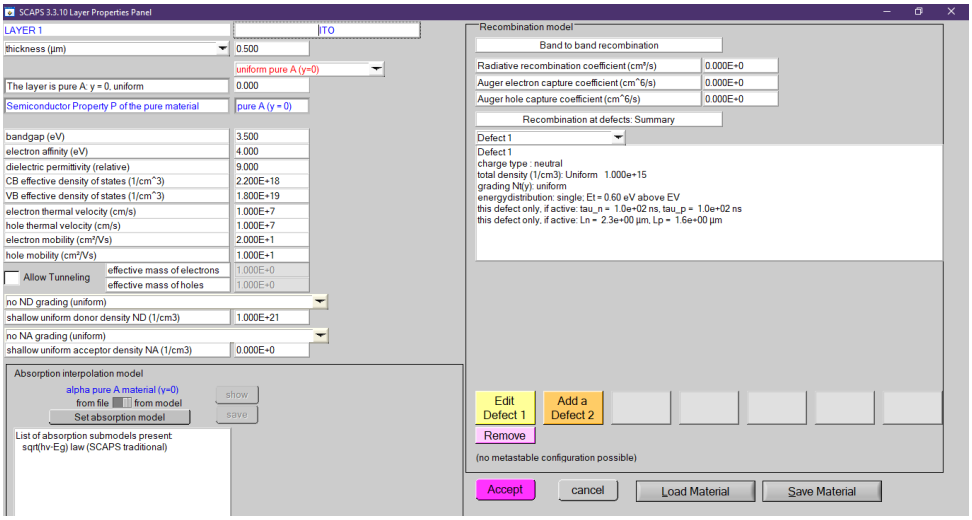

Figure 4.3: Solar Cell Definition Panel in SCAPS

4.2.4 Configuring Illumination Settings

4.4 displays the illumination settings panel in SCAPS-1D. The illumination settings panel in SCAPS-1D enables users to configure light conditions for solar cell simulations. It offers options to switch between "Dark" and "Light" modes, select spectrum files like AM1.5G, and define the illumination direction, either from the left or right. Users can also specify wavelength ranges, such as 200 nm for short and 4000 nm for long wavelengths.

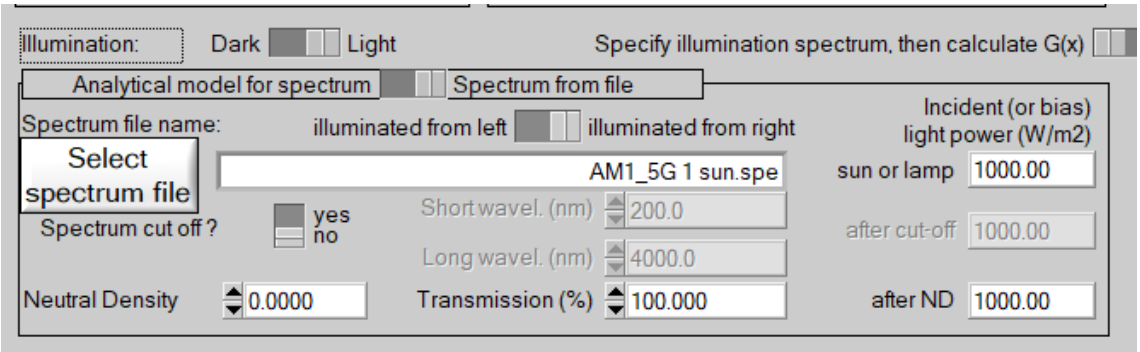

Figure 4.4: Setting Illumination Conditions

Additional features include adjusting incident light power in W/m^2, transmission percentages, and neutral density to control light intensity. The spectrum cut-off option allows limiting wavelength ranges for realistic conditions. These tools enable precise customization of illumination settings for accurate solar cell performance simulations.

4.2.5 Step-by-Step Simulation Process

(a) **Launch SCAPS**: Start the SCAPS software.

(b) **Click Input Problems**: Open the input problems section to define the simulation problem.

(c) **Set Input Parameters**: Define the solar cell's structural and material properties.

(d) **Set Working Conditions**: Configure simulation conditions, such as illumination and temperature.

(e) **Specify Actions to be Measured**: Choose the parameters to analyze (e.g., I-V, C-V).

(f) **Run the Program**: Execute the simulation to generate results.

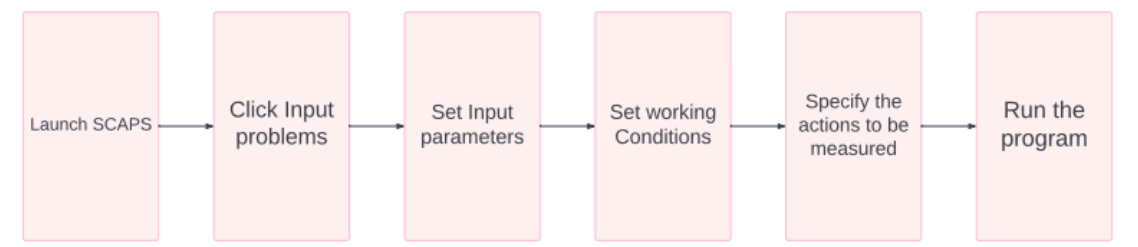

Figure 4.5: SCAPS Operating Procedure Flowchart

4.2.6 Simulated Curves

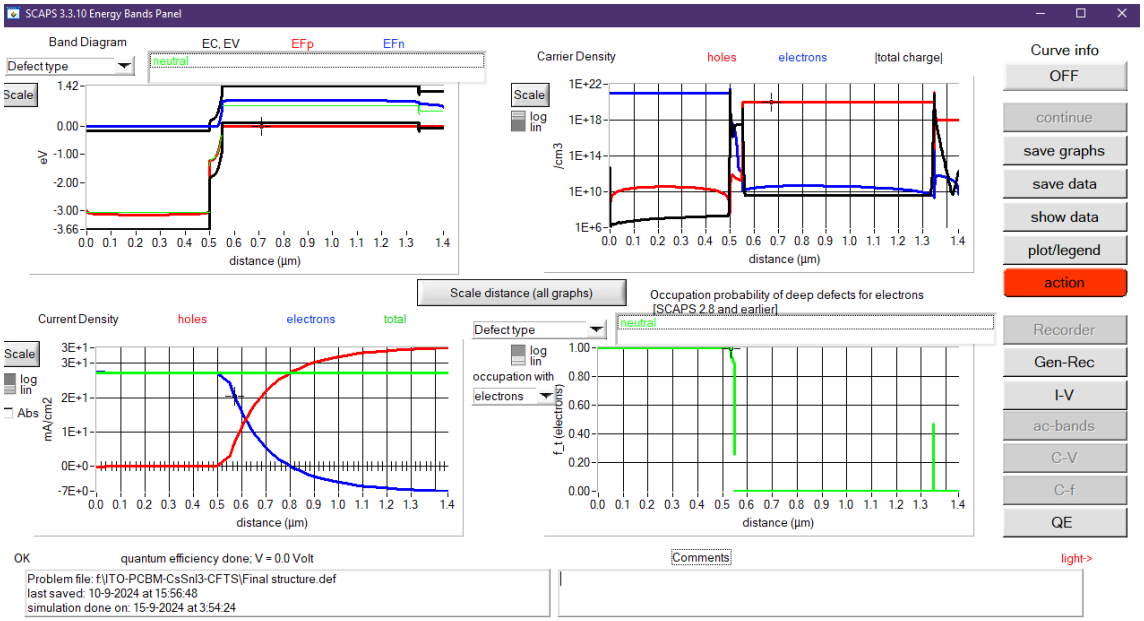

Figure 4.6: Output Display of SCAPS

After completing the calculations, SCAPS automatically navigates to the Energy Band panel, also known as the AC-band panel. This feature allows for easy examination of band diagrams, carrier densities, current densities, and other parameters at the most recently calculated bias point. If you wish to inspect an intermediate state during the computation process, you can halt the calculations early or use the pause button located in the Action Panel. The software provides multiple options for saving or displaying results: you can print them, save graphs, or display numerical values directly on the screen, which can be conveniently copied into applications like Excel or Origin. Additionally, you can switch to other output panels, such as the IV Panel, provided that you have simulated at least one corresponding measurement. Figure 4.6 presents an example of the IV Panel.

4.2.7 Proposed CsSnI3-Based Solar Cell

The simulated solar cell in this study follows a layered structure: ITO/PCBM/$CsSnI_3$/CFTS/A
The ITO layer, acting as the front contact, is exposed to sunlight, while PCBM is used as the electron transport layer (ETL). CFTS serves as the hole transport layer (HTL), and $CsSnI_3$ is the main light-absorbing material. Gold (Au) is applied as the back electrode to complete the structure. The efficiency of the photovoltaic device is influenced by several factors, including the concentration of charge carriers, temperature, cell thickness, and the optical and electrical properties of the materials. The key parameters for simulating a solar cell with $CsSnI_3$ as the absorber layer using SCAPS-1D are outlined in Table 4.1.

Figure 4.7 shows the important energy levels within the structure of the solar cell, including the lowest conduction band energy (E_C), the electron Fermi

Parameters	**ITO**	**PCBM**	**$CsSnI_3$**	**CFTS**
Thickness, (nm)	500	50	800[a]	100
Bandgap, E_g (eV)	3.5	2	1.3	1.3
Electron affinity, X (eV)	4	3.9	3.6	3.3
Dielectric permittivity, ε_r	9	3.9	9.93	9
Conduction band Density of states, N_C (cm^{-3})	2.2×10^{18}	2.5×10^{21}	1×10^{19}	2.2×10^{18}
Valance band Density of states, N_V (cm^{-3})	1.8×10^{19}	2.5×10^{21}	1×10^{18}	1.8×10^{19}
Electron mobility, μ_n (cm^2 V^{-1} s^{-1})	20	0.2	1.5×10^{3}	21.98
Hole mobility, μ_h (cm^2 V^{-1} s^{-1})	10	0.2	5.85×10^{2}	21.98
The density of p-type, N_A (cm^{-3})	0	0	10^{20}	1×10^{18}
The density of n-type, N_D (cm^{-3})	1×10^{21}	2.93×10^{17}	0	0
Density of defects, N_t (cm^{-3})	1×10^{15a}	1×10^{15a}	1×10^{15a}	1×10^{15a}

[a]In this study, these values remained constant during initial optimization to get the best combination of HTL, ETL, and Back metal contact.

Table 4.1: Defining the Input Parameters for the Simulation

energy (F_n), the hole Fermi energy (F_p), and the highest valence band energy (E_V). This diagram helps to visualize the energy states within a semiconductor or solar cell, illustrating how electrons and holes move through the different layers. The conduction band, represented by the blue line, shows the minimum energy level at which electrons are free to move. On the other hand, the red line marks the valence band, where electrons are tightly bound to atoms. The Fermi levels, shown as green lines, indicate the energy levels where electrons or holes are most likely to be found.

The gap between the conduction and valence bands, known as the band gap, plays a key role in determining how effectively a material can absorb light and convert it into electrical energy. Sharp transitions in the diagram indicate band offsets at the interfaces between layers in the solar cell. These offsets are essential for guiding the charge carriers—electrons and holes—toward the appropriate contacts, enabling the flow of electrical current that powers the solar cell.

The built-in potential that arises from the differences in energy levels within the solar cell plays a key role in efficiently separating electrons and holes. This separation helps minimize recombination losses, ultimately improving the overall efficiency of the device. The energy diagram effectively visualizes how these factors come together to enhance the solar cell's performance, enabling it to convert sunlight into usable electrical energy.

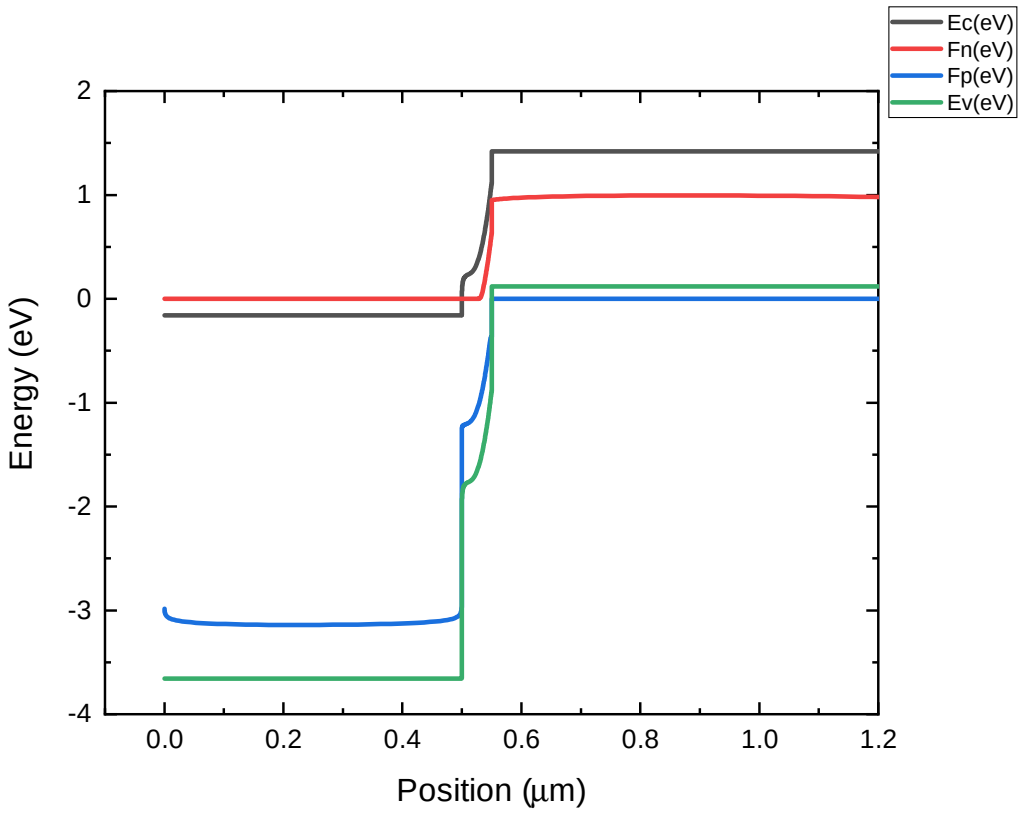

Figure 4.7: Band Diagram of Materials

To evaluate the performance of the device, SCAPS-1D simulation software was used to assess several important parameters, such as power conversion efficiency (PCE), fill factor (FF), open-circuit voltage (V_{OC}), short-circuit current density (J_{SC}), quantum efficiency (QE), and the current-voltage (J-V) characteristics. The initial results from the simulation showed an open-circuit voltage (V_{OC}) of 0.975 V, a short-circuit current density (J_{SC}) of 27.22 mA/cm^2, a fill factor (FF) of 86.97%, and a power conversion efficiency (PCE) of 23.10%. Figure 4.5 presents the J-V characteristics for the ideal MASnI device, along with the quantum efficiency curves. During the simulation, various device parameters were adjusted for optimization, including setting the thermal velocities of both electrons and holes to 10^7 cm/s.

4.3 JV Characteristics and Quantum Efficiency

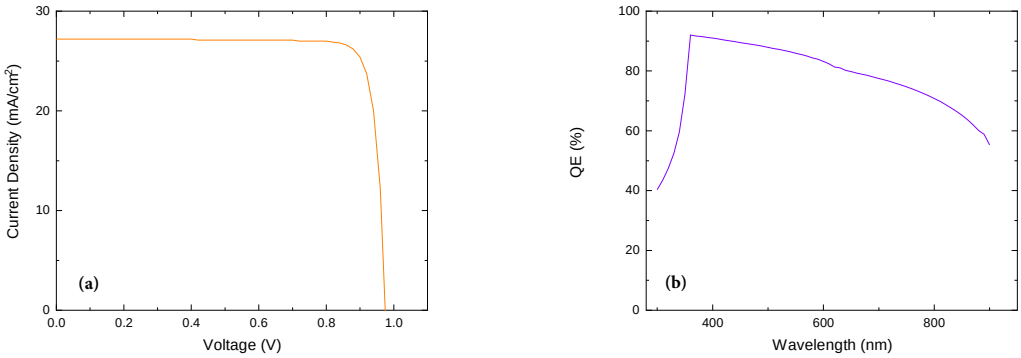

Figure 4.8: (a) $J-V$ characteristics and (b) QE curves of $CsSnI_3$ devices

The graphs in Figure 4.8 provide key insights into the performance characteristics of CsSnI devices:

1. **Graph (a): Current Density–Voltage ($J-V$) Characteristics** This graph depicts the relationship between voltage (V) on the x-axis (in volts, ranging from 0 to 1.2 V) and current density (J) on the y-axis (in mA/cm^2, ranging from 0 to 30 mA/cm^2). The curve shows how current density changes as voltage increases.

- At low voltages (near 0 V), the current density remains steady at approximately 30 mA/cm^2, indicating a high short-circuit current density (J_{sc}).
- As the voltage approaches the open-circuit voltage (V_{oc}), the current density drops sharply to zero, indicating efficient charge recombination control at this limit.
- This behavior reflects the characteristics of a well-performing solar cell, where the device generates and collects charge carriers efficiently at lower voltages, while maintaining a high V_{oc}.

2. **Graph (b): Quantum Efficiency (QE) Curve** The second graph represents the quantum efficiency (QE) of the device as a function of wavelength (λ). The x-axis shows wavelength (in nm, from 300 to 900 nm), and the y-axis displays QE in percentage (ranging from 0% to 100%).

- The QE peaks at nearly 90% in the visible spectrum, particularly between 400 and 500 nm, indicating high photon absorption and efficient charge carrier generation in this range.
- Beyond 500 nm, the QE gradually decreases, reaching its lowest values near 900 nm, reflecting the material's absorption edge, where photons lack the energy to excite electrons across the bandgap.

4.4 Impact of ITO Thickness

The figure illustrates how varying the thickness of the Indium Tin Oxide (ITO) layer affects the performance of a solar cell, focusing on Power Conversion Efficiency (PCE), Fill Factor (FF), Short-Circuit Current Density (J_{sc}), and Open-Circuit Voltage (V_{oc}). As the ITO thickness increases from 0 to 1 µm, the PCE steadily decreases from approximately 23.15% to 23.05%, due to increased optical and electrical losses, including reduced light transmission and higher series resistance.

The J_{sc} also declines, dropping from 27.33 mA/cm^2 to around 27.16 mA/cm^2, likely caused by reduced light absorption in thicker layers. Similarly, the V_{oc} decreases from about 0.98 V, reflecting increased resistive losses and diminished charge separation efficiency. In contrast, the Fill Factor (FF) shows a slight improvement, rising from approximately 86.97% with thicker ITO layers, likely due to enhanced conductivity.Overall, the results suggest that thinner ITO layers, particularly in the range of 0–0.2 µm, offer the best balance between optical transparency and conductivity.

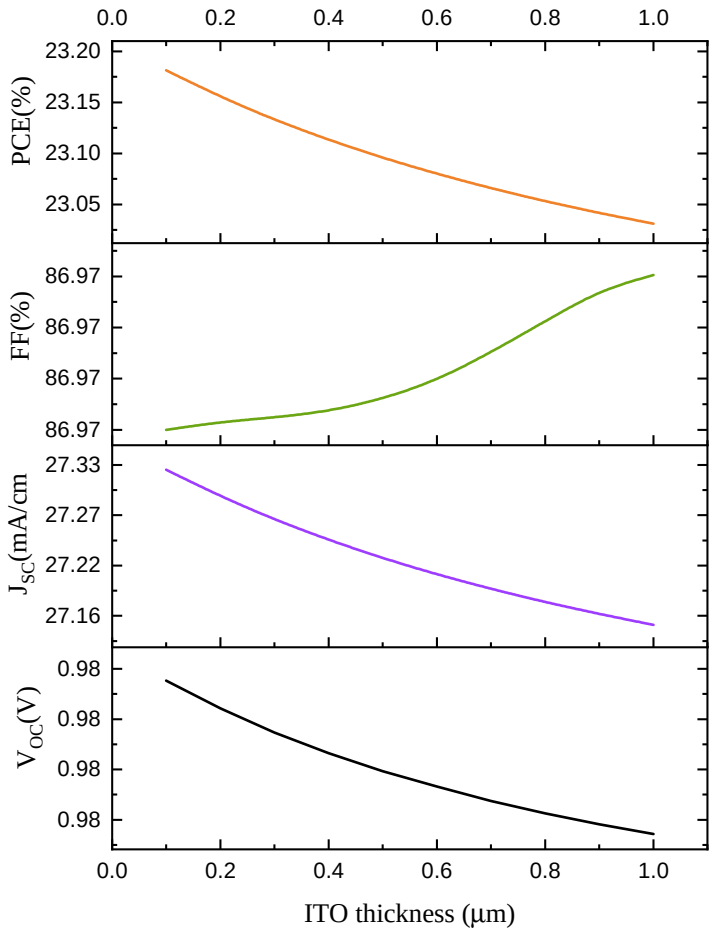

Figure 4.9: Impact of ITO Layer Thickness on Solar Cell Efficiency and Characteristics

4.5 Impact of PCBM Thickness

The graph demonstrates how the thickness of PCBM impacts four critical performance metrics of a solar cell: Power Conversion Efficiency (PCE), Fill Factor (FF), Short-Circuit Current Density (J_{SC}), and Open-Circuit Voltage (V_{OC}). As the CFTS thickness increases from 0 μm to 1.0 μm, each parameter exhibits a distinct trend.

The PCE gradually increases from approximately 23.10% at 0 μm to around 23.23% at 1.0 μm. This indicates that a thicker layer likely enhances light absorption and minimizes recombination losses, contributing to improved efficiency. The fill factor (FF), on the other hand, shows only a slight increase, remaining almost constant, with values ranging from 86.968% to 86.977%. This stability suggests that thickness has a negligible effect on resistive losses.

The short-circuit current density (J_{SC}) demonstrates a linear increase from 27.225 mA/cm^2 to 27.36 mA/cm^2, reflecting the improved light capture and charge carrier generation in thicker layers. Similarly, the open-circuit voltage (V_{OC}) increases slightly, rising from 0.9754 V to 0.9762 V, which may be attributed to better charge separation and reduced recombination.

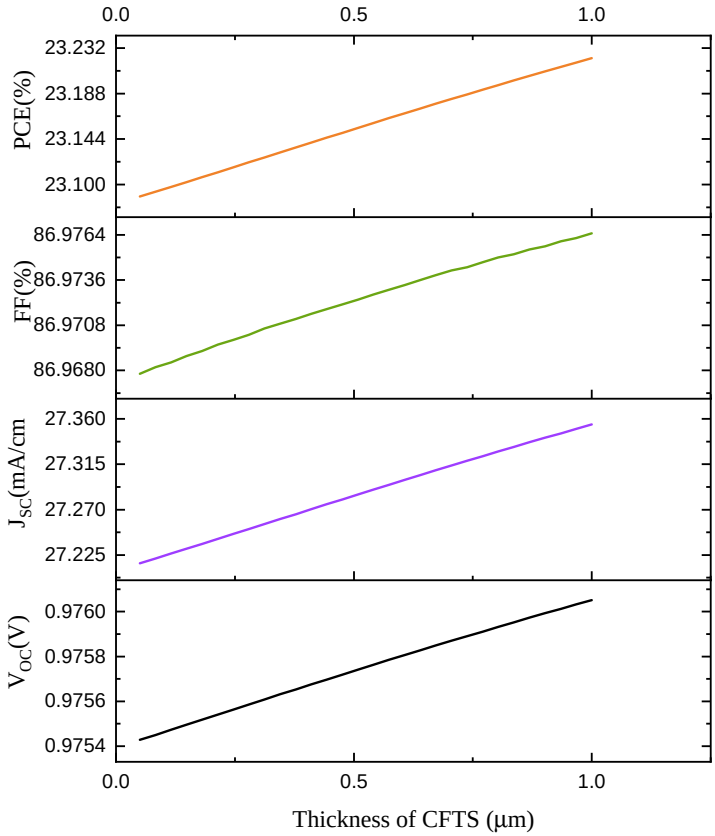

Figure 4.10: Impact of PCBM Layer Thickness on Solar Cell Efficiency and Characteristics

4.6 Impact of $CsSnI_3$ Thickness

The graph examines the relationship between the thickness of $CsSnI_3$ (in micrometers) and four key solar cell performance metrics: power conversion efficiency (PCE), fill factor (FF), short-circuit current density (J_{SC}), and open-circuit voltage (V_{OC}). As the thickness increases from 0 to 1.5 μm, the PCE shows a significant improvement, rising from approximately 17.4% to over 26.0%. This trend indicates that a thicker $CsSnI_3$ layer enhances light absorption and minimizes recombination losses, thereby improving energy conversion efficiency. Similarly, J_{SC} exhibits a clear upward trajectory, increasing from about 24 mA/cm^2 to over 30 mA/cm^2, reflecting improved photon absorption and charge carrier generation as the thickness increases.

The fill factor (FF) increases gradually from 86.5% to 87.3%, suggesting a slight reduction in resistive losses or better charge extraction efficiency. Meanwhile, V_{OC} rises steadily from 0.949 V to over 1.001 V, likely due to enhanced charge separation and reduced recombination at greater thicknesses. These findings indicate that all performance metrics benefit from increased $CsSnI_3$ thickness, with particularly strong improvements observed in PCE and J_{SC}.

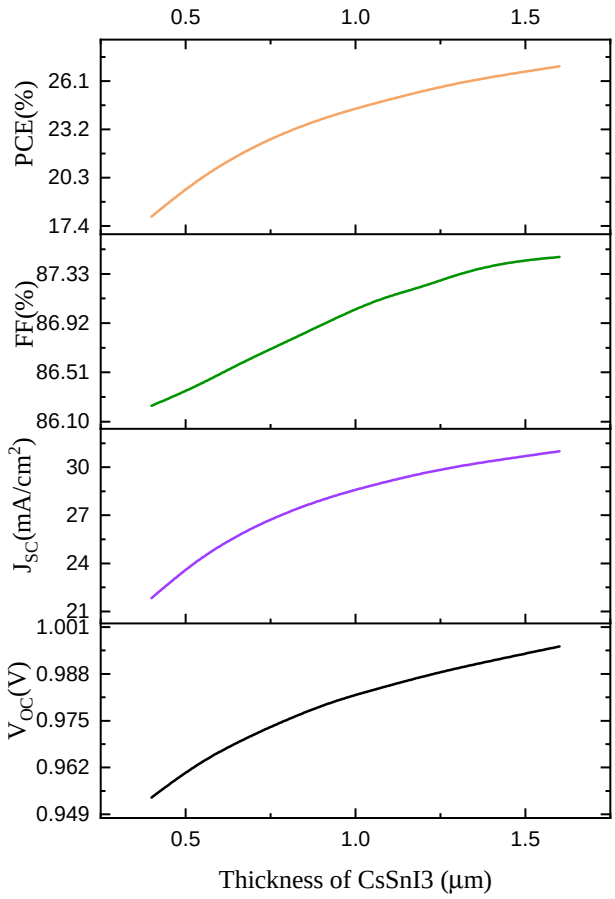

Figure 4.11: Impact of $CsSnI_3$ Layer Thickness on Solar Cell Efficiency and Characteristics

4.7 Impact of CFTS thickness

The figure demonstrates how the thickness of the CFTS (Copper Tin Sulfide) layer influences the performance of a solar cell, focusing on key parameters such as Power Conversion Efficiency (PCE), Fill Factor (FF), Short-Circuit Current Density (J_{sc}), and Open-Circuit Voltage (V_{oc}). As the thickness of the CFTS layer increases from 0 to 1 µm, a consistent improvement is observed across most metrics. The PCE rises slightly, from about 23.14% at thinner layers to approximately 23.23% at 1 µm, indicating that thicker layers improve light absorption and energy conversion efficiency. Similarly, the J_{sc} increases from 27.22 mA/cm^2 to 27.36 mA/cm^2, suggesting that a thicker CFTS layer enhances photon absorption and charge carrier generation.

The V_{oc} also shows a small but meaningful increase, starting at 0.9754 V and reaching 0.9768 V, likely due to a reduction in recombination losses. Meanwhile, the FF improves slightly, rising from 86.97% to 86.98%, indicating better charge transport and reduced resistance in thicker layers. Overall, these results highlight the importance of optimizing the CFTS layer thickness to achieve better solar cell performance. A thicker CFTS layer allows for improved light absorption and charge generation, while also minimizing recombination losses, leading to a more efficient device.

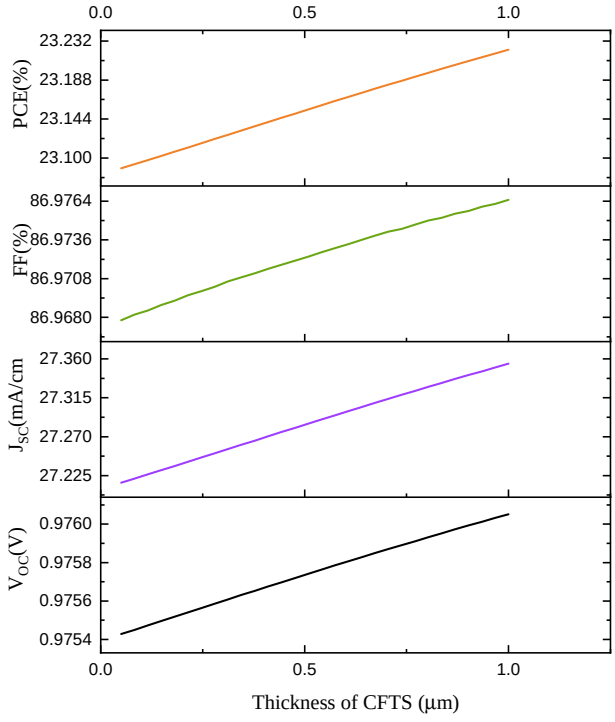

Figure 4.12: Impact of CFTS Layer Thickness on Solar Cell Efficiency and Characteristics

4.8 Impact of Electron Affinity

4.8.1 Impact of CFTS Electron Affinity on PCE (Graph a)

The first graph illustrates how the electron affinity of CFTS (Copper Tin Sulfide), used in the hole transport layer (HTL), affects the Power Conversion Efficiency (PCE) of a solar cell. The x-axis represents the electron affinity of CFTS, ranging from 3.8 eV to 4.2 eV, while the y-axis shows the PCE, ranging from around 21.6% to 23.4%. The data reveals that the PCE improves as the electron affinity increases, reaching a peak of approximately 23.4% at 4.0 eV. However, beyond this point, the PCE drops sharply, suggesting that there is an optimal electron affinity for CFTS. When the electron affinity is too low, the charge collection becomes less efficient, while excessively high electron affinity can create energy mismatches or increase recombination losses, both of which negatively affect the solar cell's performance. The table 4.3 provides the data for the changes of electron affinity for CFTS and the percentage of PCE.

Electron Affinity (eV)	**PCE (%)**
3.8	23.1958
3.91	23.2641
4.01	23.3052
4.1	23.30
4.2	21.568

Table 4.2: Power Conversion Efficiency (PCE) Variation with Different Electron Affinity Values

4.8.2 Impact of PCBM Electron Affinity on PCE (Graph b)

The second graph examines the effect of the electron affinity of PCBM (Phenyl-C61-butyric acid methyl ester), used in the electron transport layer (ETL), on the PCE of a solar cell. The x-axis represents the electron affinity of PCBM, ranging from 3.6 eV to 4.2 eV, while the y-axis displays the PCE, which varies from approximately 5.1% to 20.4%. Similar to the HTL, the PCE increases with rising electron affinity, peaking at around 20.4% near 4.0 eV. Beyond this value, the PCE declines, indicating that higher electron affinity values may cause issues such as resistive losses or energy level misalignment with other layers. Conversely, lower electron affinities result in poor electron collection, which also reduces efficiency. The results suggest that achieving the right electron affinity in the ETL is essential for effective charge transfer and minimal recombination losses.The table 4.3 provides the data for the changes of electron affinity for CFTS and the percentage of PCE.

Electron Affinity (eV)	PCE (%)
3.7	23.2255
3.8	23.1974
3.91	23.0799
4.01	22.2363
4.1	22.14

Table 4.3: Power Conversion Efficiency (PCE) Variation with Different Electron Affinity Values

4.8.3 Overall Analysis

Both graphs highlight the critical role of electron affinity in determining the efficiency of solar cells. For both the HTL (CFTS) and ETL (PCBM), the optimal electron affinity is around 4.0 eV, where the solar cell achieves its highest PCE. Deviations from this optimal value, whether lower or higher, lead to reduced efficiency due to energy mismatches, recombination losses, or poor charge transfer. These findings underline the importance of precise material design and energy level alignment in transport layers to maximize solar cell performance. Carefully engineering the electron affinities of HTL and ETL materials can significantly enhance the efficiency and reliability of the device.

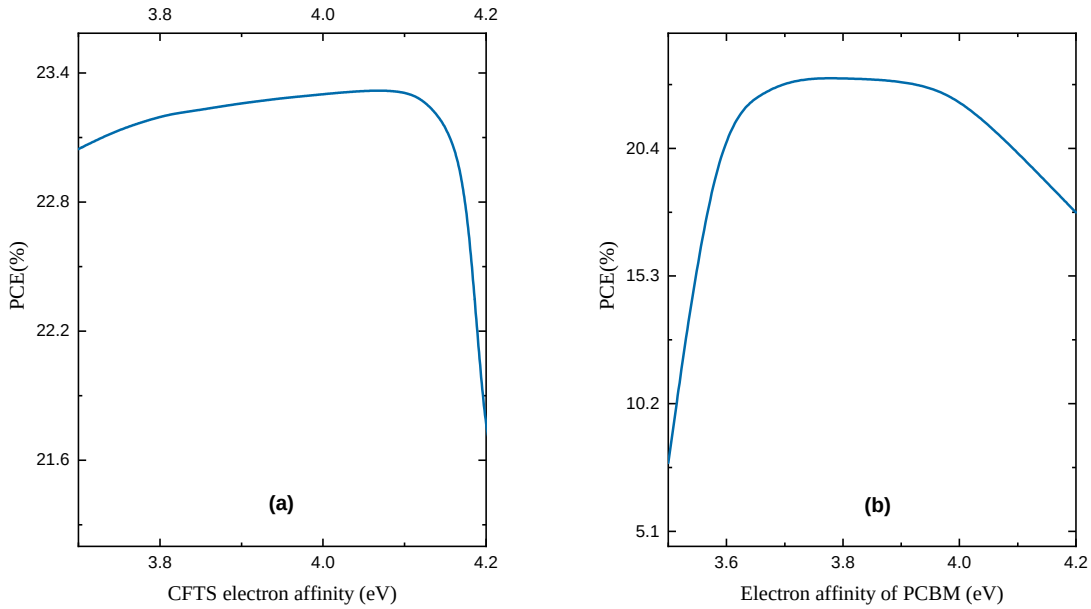

Figure 4.13: Impact of electron affinity of (a) HTL and (b) ETL on PCE.

4.9 Impact of Doping Concentration on Solar Cell parameters and Efficiency

4.9.1 Impact of Doping PCBM

Figure 4.14 shows the effect of doping concentration in PCBM (Phenyl-C61-butyric acid methyl ester) on the Power Conversion Efficiency (PCE) of a solar cell. The x-axis represents the doping concentration, measured in cm^{-3}, ranging from 0 to 1.0×10^{20}, while the y-axis displays the PCE, ranging from approximately 22.8% to 24.0%. The PCE increases steadily as the doping concentration rises, with sharper gains at lower concentrations and a gradual plateau near 24.0% as concentrations exceed $5.0 \times 10^{19}\,cm^{-3}$.

At lower concentrations, doping enhances charge carrier mobility and reduces recombination losses, significantly boosting efficiency. However, beyond a certain threshold, additional doping contributes minimally to performance improvement and can introduce resistive losses or other negative effects. The plateau at higher concentrations suggests that the material's performance is limited by intrinsic properties or interface factors. This graph underscores the importance of optimizing PCBM doping levels to maximize solar cell efficiency while avoiding over-doping and diminishing returns.

4.9.2 Impact of Doping CsSnI3

The figure shows how doping concentration in $CsSnI_3$ (Cesium Tin Iodide) affects solar cell performance metrics, including Power Conversion Efficiency (PCE), Fill Factor (FF), Short-Circuit Current Density (J_{sc}), and Open-Circuit Voltage (V_{oc}). The PCE rises from approximately 21.6% to 29.7%, plateauing at higher concentrations, while the FF improves from 82% to 89.7%, indicating better charge transport and reduced recombination losses.

Meanwhile, J_{sc} slightly decreases from 27.7 mA/cm^2 to 26.6 mA/cm^2, likely due to optical losses at higher doping levels. The V_{oc} steadily increases from 0.90 V to 1.08 V, reflecting reduced recombination and better charge separation. These results highlight the importance of optimizing doping concentrations to maximize PCE and balance gains in V_{oc} and FF with minimal impact on J_{sc}. Excessive doping leads to diminishing returns due to saturation effects and losses.

4.9.3 Impact of Doping CFTS

The graph in Figure 4.16 depicts the relationship between the doping concentration of CFTS (measured in cm^{-3}) and the power conversion efficiency (PCE) of a solar cell, expressed as a percentage. The x-axis represents the doping concentration, ranging from 0 to $1.0 \times 10^{20}\,cm^{-3}$, while the y-axis shows the PCE, which ranges from approximately 22.96% to 24.19%.

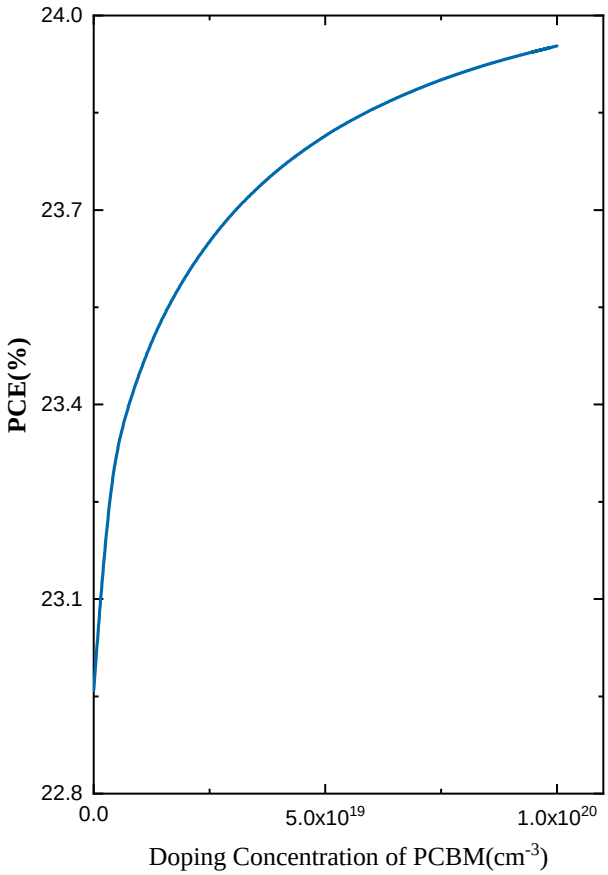

Figure 4.14: Effect of ETL Doping Concentration on Power Conversion Efficiency (PCE).

At lower doping concentrations, the PCE increases rapidly, rising from 22.96% to 24.19%. This sharp increase suggests that doping enhances the charge carrier density, improving charge transport and reducing recombination losses. The efficiency improvement reaches a turning point at around $5.0 \times 10^{19}\,\mathrm{cm}^{-3}$, after which the PCE begins to plateau. Beyond this point, further increases in doping concentration result in minimal improvements, indicating a saturation effect in the solar cell's performance. This plateau could be attributed to factors such as increased recombination or reduced carrier mobility at higher doping levels.

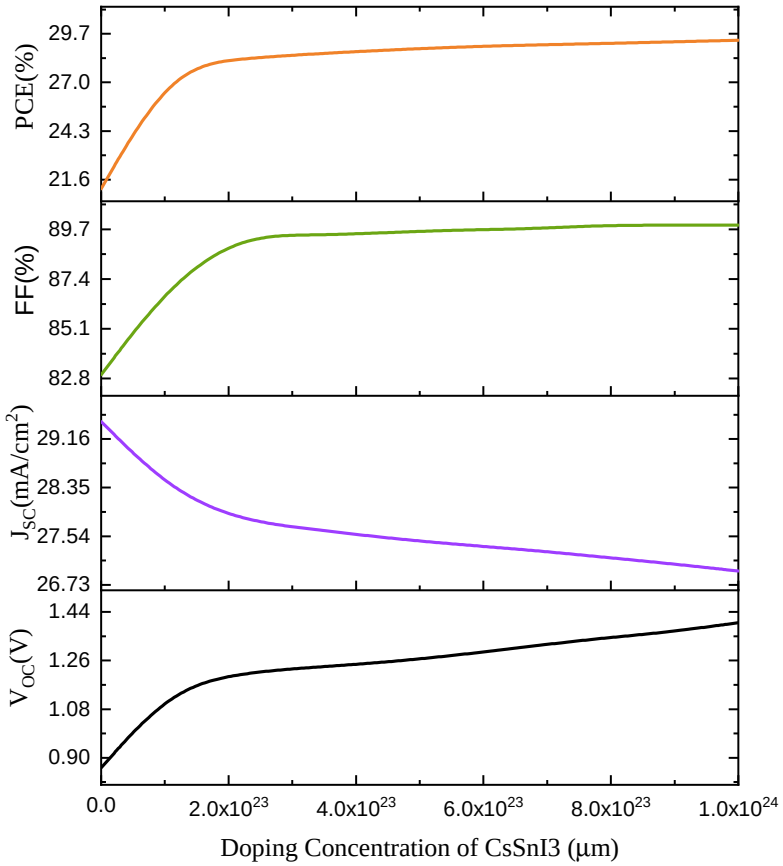

Figure 4.15: Effect of Varying Acceptor Doping Concentrations in the Absorber Layer on Solar Cell Performance

4.10 Impact of Temperature on PCE

The graph illustrates the effect of varying temperature (in Kelvin, K) on the power conversion efficiency (PCE) of a solar cell. The x-axis represents the temperature range, spanning from 280 K to 360 K, while the y-axis shows the PCE as a percentage, ranging from approximately 25.2% to 21.6%.

At the lower end of the temperature range (280 K), the PCE reaches its highest value of about 25.2%. However, as the temperature increases, the efficiency steadily declines, dropping to around 21.6% at 360 K. This negative correlation between temperature and efficiency can be attributed to factors such as increased carrier recombination, reduced carrier mobility, and thermal degradation of materials at elevated temperatures.

The findings emphasize the significance of temperature management in solar cell operation. Maintaining lower operating temperatures can help preserve efficiency and ensure stable performance. This insight is particularly important for designing solar cells to operate efficiently in environments prone to

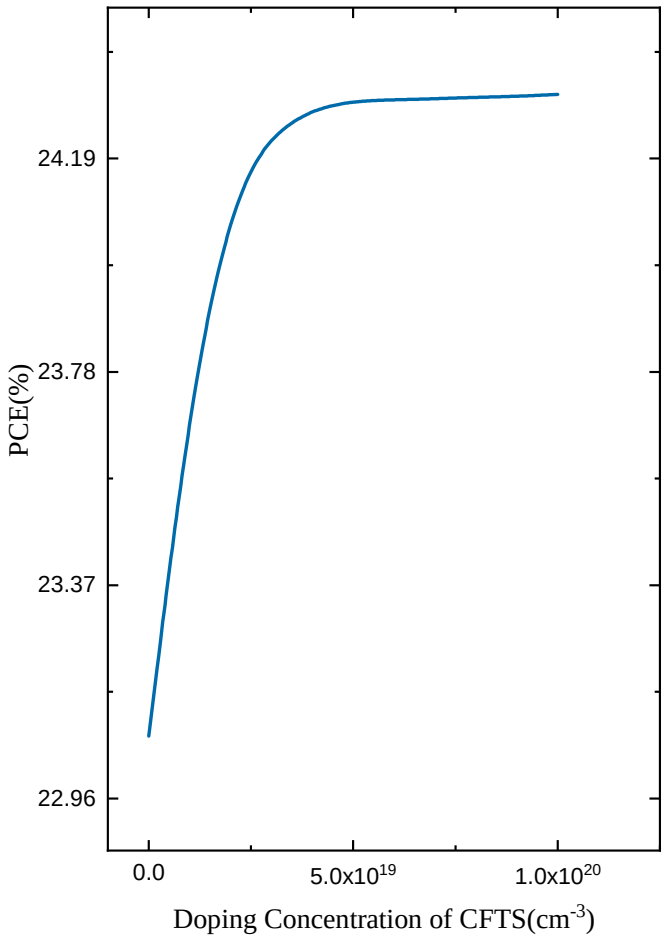

Figure 4.16: Impact of varying doping concentration of HTL on PCE.

higher temperatures.

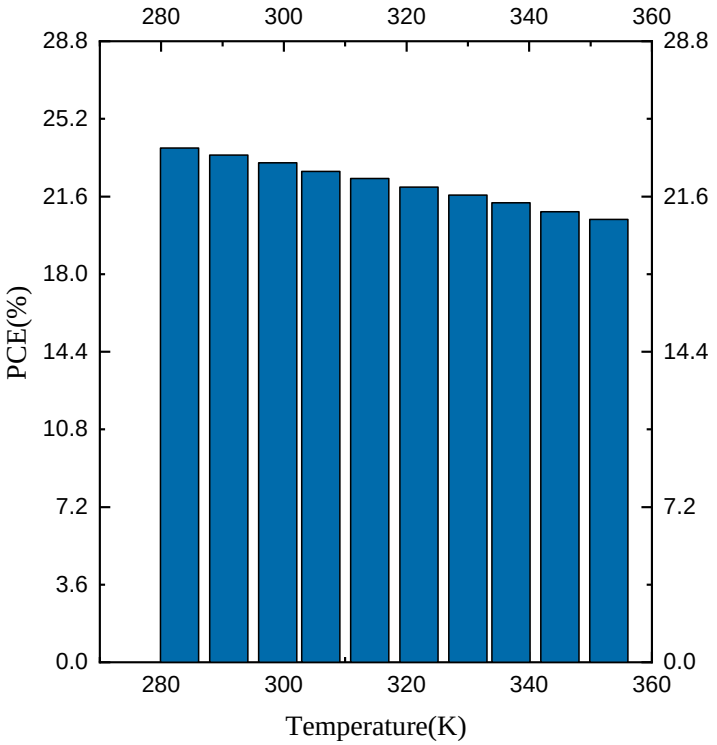

Figure 4.17: Impact of varying Temperature on PCE.

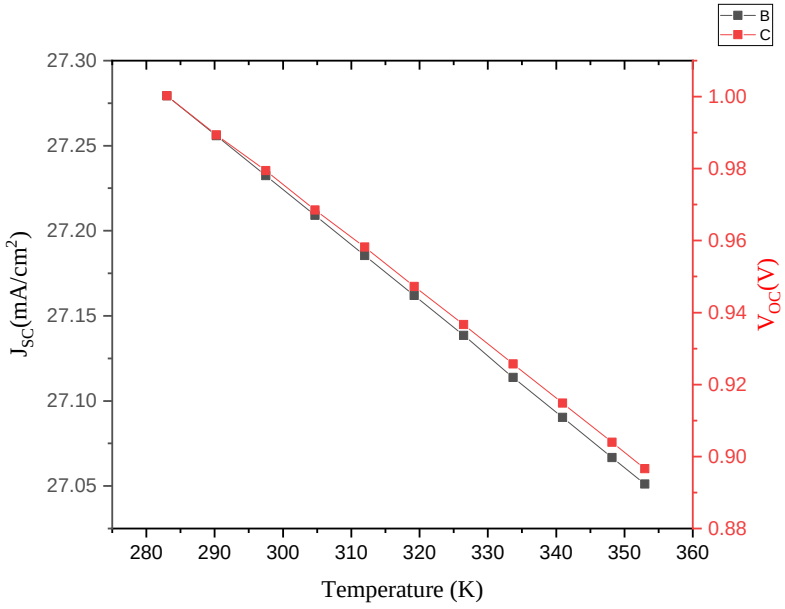

Figure 4.18: Impact of varying Temperature on J_{SC} and V_{OC}.

The graph illustrates how temperature affects two key performance parameters of a solar cell: the Short-Circuit Current Density (J_{sc}) and the Open-Circuit Voltage (V_{oc}). The x-axis represents temperature, ranging from 280 K to 360 K, while J_{sc} is displayed on the left y-axis in mA/cm^2, and V_{oc} is shown on the right y-axis in volts. As temperature increases, J_{sc} shows a slight decrease,

dropping from about 27.30 mA/cm^2 at 280 K to approximately 27.05 mA/cm^2 at 360 K. This decline is due to reduced charge carrier mobility and increased recombination losses at elevated temperatures.

Similarly, V_{oc} decreases more significantly, starting at around 1.00 V at 280 K and dropping to roughly 0.88 V at 360 K. This drop occurs because higher temperatures enhance carrier recombination and reduce the energy gap between the quasi-Fermi levels. The graph highlights the negative impact of rising temperatures on solar cell performance, emphasizing the importance of temperature control to maintain efficiency and functionality in practical applications.

4.11 Analysis of Optimized Result

The highest efficiency for the CsSnI solar cell was reached through precise optimization of several essential parameters that directly influenced its performance. The absorber layer was specifically designed with a thickness of 1.6 micrometers to maximize light absorption, while the Indium Tin Oxide (ITO) layer, serving as a transparent conductive electrode, was finely tuned to a thickness of 0.1 micrometers. Additionally, the hole transport layer (HTL) was crafted at 1 micrometer to facilitate smooth and efficient charge transport across the cell.

The electron affinities of the charge transport layers were carefully selected, with one CTFS layer set at 4.1 eV and another at 3.7 eV. To ensure effective light absorption and optimal charge carrier generation, the absorber layer was doped to a concentration of $2.0 \times 10^3\,\mathrm{cm}^{-3}$. The HTL's doping concentration was adjusted to $5 \times 10^{19}\,\mathrm{cm}^{-3}$, while the electron transport layer (ETL) was maintained at $1.0 \times 10^2\,\mathrm{cm}^{-3}$.

These adjustments were all carried out at a temperature of 283 K, leading to a notable efficiency of 26.9%. This carefully balanced combination of layer thicknesses, doping concentrations, and electron affinities underscores the importance of fine-tuning in creating high-performance CsSnI solar cells and highlights how such precision can drive significant improvements in energy conversion efficiency.

Bibliography

[1] A. Rohatgi, "High-efficiency silicon solar cells opportunity and challenge," in *Proceedings of SPIE*, SPIE, Aug. 1985. DOI: 10.1117/12.948191. [Online]. Available: https://doi.org/10.1117/12.948191.

[2] M. A. Green, "Photovoltaics: Technology overview," *Energy Policy*, vol. 28, no. 14, pp. 989–998, Nov. 2000. DOI: 10.1016/s0301-4215(00)00086-0. [Online]. Available: https://doi.org/10.1016/s0301-4215(00)00086-0.

[3] F. Pfisterer, *Photovoltaic cells*, Jun. 2000. [Online]. Available: https://onlinelibrary.wiley.com/doi/10.1002/14356007.a20_161.

[4] *Scientific principles*, Accessed: [Insert access date here], Jan. 2000. [Online]. Available: https://matse1.matse.illinois.edu/sc/prin.html.

[5] T. Lai and H. Lee, "Development of semiconductor and superconductor technology and future bioscience," *World Scientific*, vol. 16, no. 05, pp. 283–293, Oct. 25, 2004. DOI: 10.4015/s1016237204000402.

[6] K. Gokhberg and L. S. Cederbaum, "Environment assisted electron capture," *IOP Publishing*, vol. 42, no. 23, pp. 231 001–231 001, Nov. 2009. DOI: 10.1088/0953-4075/42/23/231001.

[7] P. Fulay and J.-K. Lee, *Electronic, Magnetic, and Optical Materials*. CRC Press, 2010. [Online]. Available: https://www.taylorfrancis.com/books/mono/10.1201/9781439882603/electronic-magnetic-optical-materials-pradeep-fulay-jung-kun-lee.

[8] *P-n junctions*, Accessed: [Insert access date here], Jan. 2011. [Online]. Available: https://www.pveducation.org/pvcdrom/p-n-junctions.

[9] R. Berger and J. B. Neaton, *Design of low band gap double perovskites from first principles*, Cornell University, Jan. 2012. DOI: 10.48550/arXiv.1209.

[10] C. Morcillo-Herrera, F. Hernández-Sánchez, and M. Flota-Banũelos, "Practical method to estimate energy potential generated by photovoltaic cells: Practice case at merida city," *Energy Procedia*, vol. 57, pp. 245–254, Jan. 2014. DOI: 10.1016/j.egypro.2014.10.029. [Online]. Available: https://doi.org/10.1016/j.egypro.2014.10.029.

[11] J. Chen, "Recent developments on silicon based solar cell technologies and their industrial applications," Apr. 2015. DOI: 10.5772/59171.

[12] N. Amin, S. A. Shahahmadi, P. Chelvanathan, K. S. Rahman, M. I. Hossain, and M. Akhtaruzzaman, "Solar photovoltaic technologies: From inception toward the most reliable energy resource," in *Comprehensive Renewable Energy*, Elsevier BV, Jan. 2017, pp. 11–26. DOI: 10.1016/b978-0-12-409548-9.10092-2. [Online]. Available: https://doi.org/10.1016/b978-0-12-409548-9.10092-2.

[13] D. Zhou, T. Zhou, Y. Tian, X. Zhu, and Y. Tu, "Perovskite-based solar cells: Materials, methods, and future perspectives," *Hindawi Publishing Corporation*, vol. 2018, pp. 1–15, Jan. 2018. DOI: 10.1155/2018/8148072.

[14] A. C. Nkele, A. C. Nwanya, N. M. Shinde, *et al.*, "The use of nickel oxide as a hole transport material in perovskite solar cell configuration: Achieving a high performance and stable device," *International Journal of Energy Research*, vol. 44, no. 13, pp. 9839–9863, Jun. 2020. DOI: 10.1002/er.5563. [Online]. Available: https://doi.org/10.1002/er.5563.

[15] A. A. E. O. Sarradj, *Analysis and design of photovoltaic systems*, Master's Thesis, University of Biskra, 2022. [Online]. Available: http://archives.univ-biskra.dz/bitstream/123456789/21729/1/SARRADJ_AYMEN_ABD_EL_OUADOUD.pdf.

[16] F. Author, "Title of the dissertation," PhD Dissertation, Ph.D. dissertation, Institution Name, 2023. [Online]. Available: https://www.proquest.com/docview/3073252930.

[17] P. K. Sonkar and V. Ganesan, Eds., *Advancements in Nanomaterials for Energy Conversion and Storage*. CRC Press, 2023. [Online]. Available: https://www.taylorfrancis.com/books/edit/10.1201/9781003481157/advancements-nanomaterials-energy-conversion-storage-piyush-kumar-sonkar-vellaichamy-ganesan.

[18] M. C. Langveld and J. J. Clark, *Economics of solar energy*, Accessed: [Insert access date here]. [Online]. Available: https://journals.sagepub.com/doi/10.1177/001088047601600412.

[19] *Electrons, photons, and the photo-electric effect*, Accessed: [Insert access date here], n.d. [Online]. Available: https://physics.bu.edu/py106/notes/PhotoelectricEffect.html.

[20] Particle Data Group, *Review of Particle Physics: Photon and Electron*, Retrieved from urlhttps://pdg.lbl.gov/1998/photonelecrppbook.pdf, n.d.

[21] *Photodiode characteristics and applications*, Retrieved from urlhttp://www.osioptoelectronics.com/application-notes/an-photodiode-parameters-characteristics.pdf, n.d.

[22] *Photoelectric effect*, Accessed: [Insert access date here], n.d. [Online]. Available: https://vallance.chem.ox.ac.uk/pdfs/PhotoelectricEffect.pdf.

[23] *Semiconductor materials*, Accessed: [Insert access date here], n.d. [Online]. Available: https://www.pveducation.org/pvcdrom/pn-junctions/semiconductor-materials.

[24] *Solar cell structure — pveducation*, Accessed: [Insert access date here], n.d. [Online]. Available: https://www.pveducation.org/pvcdrom/solar-cell-operation/solar-cell-structure.

[25] Zeman, *Microsoft word - ch4 solar cell operational principles.doc*, Retrieved from urlhttps://ocw.tudelft.nl/wp-content/uploads/Solar-Cells-R4-CH4$_S olar_c ell_o perational_p r$ n.d.